Investigation of particle effects on bubble coalescence in slurry with a chimera MP-PIC and VOF coupled method

Liao, Y.; Wang, Q.; Caliskan, U.; Miskovic, S.;

Originally published:

October 2022

Chemical Engineering Science 265(2023), 118174

DOI: https://doi.org/10.1016/j.ces.2022.118174

Perma-Link to Publication Repository of HZDR:

https://www.hzdr.de/publications/Publ-34914

Highlights

Investigation of particle effects on bubble coalescence in slurry with a chimera MP-PIC and VOF coupled method

Yixiang Liao,Qingdong Wang,Utkan Caliskan,Sanja Miskovic

- Film drainage and bubble coalescence is investigated with high-resolution numerical methods.
- Effect of particles and their properties on thin liquid film drainage and rupture is studied in detail.
- The influence of particle concentration on the coalescence time in co-axial cases is multmodal.
- Particles may block coalescence, change drainage axisymmetry and affect film instability.
- Wake entrainment is a key factor influencing coalescence in bubble columns.

Investigation of particle effects on bubble coalescence in slurry with a chimera MP-PIC and VOF coupled method

Yixiang Liao[a,*], Qingdong Wang[a], Utkan Caliskan[b] and Sanja Miskovic[b]

[a]Helmholtz-Zentrum Dresden-Rossendorf, Institute of Fluid dynamics, Bautzner Landstraße 400, 01328 Dresden, Germany
[b]Norman B. Keevil Institute of Mining Engineering, University of British Columbia, 2329 West Mall, Vancouver, BC V6T 1Z4, Canada

ARTICLE INFO

Keywords:
Bubble coalescence
Chimera grid
MP-PIC and VOF coupled
Particle effects
Slurry

ABSTRACT

Bubble coalescence and breakup is still a complex challenging topic. How far it is understood affects directly the analysis and design optimization of multiphase reactors. Despite years of active research, bubble coalescence in three-phase systems is far from being understood. Contradictory results on the effect of particles are often reported. Although it still lacks a unique explanation, a general conjecture is that the presence of solid particles affects the film drainage process, and hence the bubble coalescence time and behaviour. This paper presents insights into bubble-pair coalescence in slurry by coupling the multiphase particle in cell (MP-PIC) method with the volume of fluid (VOF) method. The mesh resolution for VOF fields is down to micrometers, which allows for analysis of the film drainage and rupture mechanism in detail. The accuracy of MP-PIC fields during the refinement of CFD grids is guaranteed by a chimera approach (Caliskan and Miskovic, Chemical Engineering Journal Advances 5 (2021) 100054), which allows two overlapping meshes in the Lagrangian-Eulerian framework, namely, a fine mesh for the CFD fields and a coarser mesh for the MP-PIC ones.

1. Introduction

Gas-liquid-solid systems are commonly encountered in chemical, biological, coal and mineral process industry as well as wastewater treatment and environmental pollution abatement devices (Krishna and Sie, 2000; Kumar et al., 1993; Wu and Gidaspow, 2000). In these circumstances, gas bubbles and their motion play an essential role in determining the performance of the system or process, and therein bubble coalescence is a major mechanism affecting the bubble size, and correspondingly the hydrodynamics. Bubble coalescence is substantially complicated due to the presence of particles. Despite years of active research, bubble coalescence in three phase systems is far from understood. Contradictory results on the particle effects are often reported (Banisi et al., 1995; Bhunia et al., 2017; Bukur et al., 1990; Khare and Joshi, 1990; Ojima et al., 2014; Tavera and Escudero, 2012; Vazirizadeh, 2015). A general conjecture is that the presence of solid particles affects the film drainage process and hence the bubble coalescence behaviour (Gandhi, 1998; Hooshyar et al., 2010; Vazirizadeh, 2015). Quantitative data for a conclusive remark and general mathematical description are, however, lacking, and further investigations are necessary. Jamialahmadi and Müller-Steinhagen (1991) stated that the existence of hydrophilic particles in the liquid film may increase the resistance to film drainage and bubble coalescence due to the repulsive forces between the particles and the bubbles. On the other hand, Omota et al. (2005) suggested that if relative motion between particles and liquid as well as particle-induced turbulence is noticeable, particles may destabilize the liquid film and enhance the coalescence of bubbles. It has been evidenced as well that the approach velocity of the bubbles has a significant impact on the deformation and film drainage process and consequently the coalescence (Horn et al., 2011; Zhang, 2017). Most investigations on film drainage and bubble coalescence in presence of particles were performed under very low approach velocity (up to 0.1 mm/s), where the hydrodynamic effects are negligible (Ata, 2008; Gallegos-Acevedo et al., 2010; Spyridopoulos et al., 2004). Studying such interactions under hydrodynamic conditions with high approach velocity, e.g. during free rising, is highly preferred since it covers many practical problems encountered in industrial processes. Computational fluid dynamics (CFD) has been proven to be capable of providing insights into local flow phenomena as a supplement to experimental capabilities, and is becoming an increasingly important tool in the design, scale-up and optimization of multiphase reactors or processes (Koh and Schwarz, 2006; Salem-Said et al., 2013). The accuracy of multi-fluid CFD simulation for three-phase flows, which is mostly used because of lowest computational costs, is degraded greatly

*Corresponding author
y.liao@hzdr.de (Y. Liao)

due to insufficient knowledge on the mechanism of bubble coalescence in presence of particles. Recently, bubble size distribution instead of a constant bubble size is often considered by coupling the CFD with a population balance model (PBM), which provides a possibility to take into account bubble coalescence as well as particle effects. The simulation based on this approach is referred to as a CFD-PBM coupled simulation, which represents however still a huge challenge for three-phase systems. One major reason is that no reliable models are available for the description of particle effects on bubble coalescence. The models developed for two-phase systems are used commonly to close the population balance equation without any justification. For example, the Luo (1993) model, which was developed for gas-liquid or liquid-liquid dispersions, has been adopted in Chen et al. (2004); Syed (2017); Troshko and Zdravistch (2009); Xu et al. (2014) for slurry bubble columns, and the Prince and Blanch (1990) model in Basha and Morsi (2018); Rabha et al. (2013a); Sarhan et al. (2018). Both models are based on the film drainage theory, and the coalescence efficiency has a common form of

$$P_c(d_i, d_j) = exp(-CWe_{ij}^{0.5}), \tag{1}$$

where d_i, d_j is the diameter of the bubble i and bubble j, the Weber number We_{ij} defined in terms of the approach velocity between the two bubbles and their equivalent size. There is no general expression for the pre-factor C even for gas-liquid two-phase systems. According to Prince and Blanch (1990) it depends on the natural logarithm of the ratio of the initial film thickness and critical film thickness where rupture occurs, while in the model of Luo (1993) it is related further to the density ratio of gas to liquid, bubble size ratio as well as virtual mass coefficient, and Liao et al. (2014) treat it simply as an adjustable constant. But in general they all are insufficient for the description of bubble coalescence in presence of particles, since the particle-effect is not considered at all, which in the opposite has been experimentally demonstrated (Banisi et al., 1995; Bhunia et al., 2017; De Swart et al., 1996; Gandhi, 1998; Ghani et al., 2012; Hooshyar et al., 2010; Jamialahmadi and Müller-Steinhagen, 1991; Kara et al., 1982; Krishna and Sie, 2000; Ojima et al., 2014; Rabha et al., 2013b; Su, 2005; Tavera and Escudero, 2012; Vandu et al., 2004; Vazirizadeh, 2015). To the best of the authors' knowledge Ojima et al. (2014) were the first to take into account the reduction effect of hydrophilic particles on the coalescence time observed in their experiments. They correlated the coalescence time in terms of particle concentration based on the data for a 2D slurry bubble column, and implemented the effect as a modification factor β in the Prince and Blanch (1990) model, i.e.

$$P_c(d_i, d_j) = exp(-\beta CWe_{ij}^{0.5}), \tag{2}$$

where β is evaluated using linear interpolation between the limits of $\beta = 1.0$ at $C_s = 0$ and $\beta = 0.0$ at $C_s = 0.45$ (C_s is the particle volumetric concentration). The good agreement on gas holdup in a slurry bubble column using the modified model evidences that it is possible to simulate bubble coalescence in three-phase systems reliably by updating the models that originally developed for two-phase systems. However, more fundamental research on the mechanism of particle effects and derivation of a physically-based modification factor are necessary.

The particle effects on the bubble coalescence can be well-captured using a Eulerian-Lagrangian based modeling approach such as CFD-DPM-VOF (Liu and Luo, 2018). In this study, another Eulerian-Lagrangian method called the Multiphase Particle in Cell (MP-PIC) method is used (Snider, 2001). The difference between the CFD-DEM-VOF and CFD-MPPIC-VOF is in the particle collision modeling where the former calculates particle-particle interaction directly, whilst the latter resolves the particle positions on the cell scale by using the averaged particle properties on the Eulerian mesh created through an interpolation method. The Eulerian field values are also interpolated from the mesh back to the particles for particle interaction calculations. The DEM method is more accurate in comparison to the MP-PIC method (Li and Eri, 2021), but the modeling of the particle interactions in the MP-PIC is computationally much more efficient than the DEM method. Secondly, the MP-PIC can employ a parcel concept where a number of particles are grouped into one parcel to increase computational efficiency. Furthermore, Numerous studies demonstrated coupled CFD-DEM-VOF models, i.e (He et al., 2020; Jing et al., 2016; Liu and Luo, 2018; Pozzetti et al., 2019; Pozzetti and Peters, 2018), and relatively fewer for MP-PIC-VOF models (Kumar et al., 2021). The coupling strategy for both approaches can be identical and in the MP-PIC, the accuracy of the coupling can be improved with high-order interpolation methods. The default coupling strategy in OpenFOAM is the simplest; in other words, the coupling terms, such as momentum exchange term and the porosity, are created by adding the particle property to the belonging cell without considering the possible overlap of the particle to a neighboring cell. That can be less troublesome for CFD-DEM applications but problematic for MP-PIC due to a possible staggering of particles since the MP-PIC does not guarantee non-overlapping between particles. The direct resolution of the particle interactions in CFD-DEM prevents

such behavior. The coupling strategies for the CFD-DEM-VOF approach are well-documented in the literature, and those can be notable references to the MP-PIC-VOF approach. The MP-PIC method is practical for dense particulate flows because of its fast particle collision modeling and scalability by employing a parcel approach. Moreover, the VOF coupling to the model can provide an accurate solution to large-scale three-phase solid-liquid-gas flow modeling. Such systems are seen in industries that involve hydraulic solid particles transportation and processing such as mining, oil, and gas, agriculture, and waste treatment.

The main objective of this study is to acquire insights into bubble coalescence behavior in presence of insoluble hydrophilic particles by means of high-resolution CFD simulations. The coalescence of bubble pairs under different particle size, density and concentration is investigated in OpenFOAM v8 using the multiphase particle-in-cell (MP-PIC) and volume of fluid (VOF) coupled method, with the consideration of its good efficiency, since the particle concentration in the investigated cases is relatively high. The remainder of this paper is structured as follows. In Section 2 the numerical approach is introduced in great detail, while its validation for various conditions is presented in Section 3. The investigated cases and results on the particle effects are discussed in Section 4, and finally a brief summary in Section 5 concludes the paper.

2. Numerical method

Multiphase particle-in-cell (MP-PIC) (Wikipedia, 2010) is a numerical method for modeling particle-fluid and particle-particle interactions in a CFD calculation. In the coupled approach, the particle properties are mapped from the Lagrangian coordinates to an Eulerian grid through the use of interpolation functions. After evaluation of the continuum derivative terms like volume fraction and velocity field, the particle properties are mapped back to the individual particles along with updated interaction forces. The MP-PIC method has proven to be numerically stable and computationally efficient for dense particle flows because it simultaneously treats the particles as computational particles and as a continuum by mapping the averaged particle fields on the Eulerian mesh, and resolving particle-particle interactions using those averaged fields. (Snider, 2001).

2.1. Governing Equations for the Eulerian Phase

The MPPICInterFoam solver in OpenFOAM v8 is adopted in this study, where the Eulerian phase, i.e. the gas and liquid mixture, is simulated using the VOF method, which employs the MULES (Multidimensional Universal Limiter for Explicit Solution) method. The algorithm of the MULES method for interface tracking is explained in detail in Márquez Damián (2013).The governing equations of the coupled MP-PIC-VOF model are summarized in the following.

Continuity equation:

$$\frac{\partial \alpha_c}{\partial t} + \nabla \cdot (\boldsymbol{\alpha_c U}) = 0 \tag{3}$$

Alpha transport equation:

$$\frac{\partial (\alpha_c \alpha)}{\partial t} + \nabla \cdot (\alpha_c \alpha \boldsymbol{U}) + \nabla \cdot (\alpha_c \alpha (1-\alpha) \boldsymbol{U}_c) = 0, \tag{4}$$

where α_c is the volume fraction of fluids, namely, 1 - α_p, with α_p standing for the particle volume fraction, and α denotes the volume fraction of the primary phase, liquid in this study. The last term in Eq. 4 is an artificial compression term, which is introduced for the sharpening of the gas-liquid interface, and $\boldsymbol{U_c}$ represents the compression velocity. In comparison to the MPPICInterFoam solver of OpenFOAM where α_c in the time derivative term of the alpha-equation is neglected, the MPPIC-VOF solver in this study involves a volume-conservative solution of the alpha transport equation due to the transient change of the local porosity, namely, the void fraction of the continuous phase. This is implemented within the semi-implicit solution of the MULES method. In other words, Eq. 4 conserves the volume fraction of the liquid (α) due to the motion of particles as they enter or exit the liquid.

Momentum equation:

$$\frac{\partial (\alpha_c \rho \boldsymbol{U})}{\partial t} + \nabla \cdot (\alpha_c \rho \boldsymbol{U}\boldsymbol{U}) = -\nabla P + \nabla \cdot (\alpha_c \boldsymbol{\tau}) + \alpha_c \rho \boldsymbol{g} + \boldsymbol{f}_\sigma + \boldsymbol{F} \tag{5}$$

where $\boldsymbol{f}_\sigma$ is the surface tension force, and the term $\boldsymbol{F}$ is defined as the average momentum transfer between the fluid and the particles in a unit volume (Verma and Padding, 2020). It becomes negligible as the fluid volume fraction α_c approaches unity or $\alpha_p \approx 0$.

2.2. Governing Equations for the Particle Phase

The particle phase is described by a probability distribution function, $f(\boldsymbol{x}, \boldsymbol{U}_p, \rho_p, \Omega_p, t)$, which indicates the likelihood of a particle with velocity $\boldsymbol{U}_p$, density ρ_p, volume Ω_p present at the location $\boldsymbol{x}$ and time t. In the case of no volumetric source and sink terms, the transport equation is expressed as

$$\frac{\partial f}{\partial t} + \nabla \cdot (f \boldsymbol{U}_p) + \nabla_{\boldsymbol{U}_p} \cdot (f \boldsymbol{A}_p) = 0 \tag{6}$$

The transportation is coupled with the fluid phase through the particle acceleration term, $\boldsymbol{A}_p$, which is defined as

$$\boldsymbol{A}_p = D_p(\boldsymbol{U} - \boldsymbol{U}_p) + \frac{\rho}{\rho_p}\left[\frac{D\boldsymbol{U}}{Dt}\right]_p + \boldsymbol{g}\left(1 - \frac{\rho}{\rho_p}\right) - \frac{\nabla \tau_p}{\alpha_p \rho_p}, \tag{7}$$

where the coefficient $\boldsymbol{D}_p$ is determined from a model for the dimensionless drag coefficient $\boldsymbol{C}_D$. The pressure gradient term is modified into two terms, the local acceleration term interpolated to the location of particle p, and buoyancy force: $\left[\frac{D\boldsymbol{U}}{Dt}\right]_p - g\ \frac{\rho}{\rho_p}$. The combination of the Ergun (Ergun, 1952) and Wen-Yu (Wen, 1966) drag correlations is adopted in this study (Caliskan and Miskovic, 2021).

$$D_p = \begin{cases} 150\frac{\mu_c \alpha_p}{\rho_p \alpha_c^2 d_p^2} + 1.75\frac{\rho|U - U_p|}{\alpha_c \rho_p d_p}, & \alpha_c < 0.8 \\ C_D \frac{3}{4}\frac{\alpha_c \rho\ |U - U_p|}{\alpha_c \rho_p d_p}\alpha_c^{-2.7}, & \alpha_c \geq 0.8 \end{cases} \tag{8}$$

$$C_D = \begin{cases} \frac{24\left(1 + 0.15 Re_p^{0.687}\right)}{Re_p}, & Re_p < 1000 \\ 0.44, & Re_p \geq 1000 \end{cases}, \quad Re_p = \frac{\alpha_c\ \rho\ d_p \left|U - U_p\right|}{\mu_c} \tag{9}$$

where μ_c is the dynamic viscosity of the continuous phase, and d_p is the particle diameter.

In the MP-PIC method, the description of particle-particle collision is simplified by introducing a continuum stress term τ_p (see Eq. (7)). According to the model of Harris and Crighton (1994), it is expressed as

$$\tau_p = \frac{P_s \alpha_p^{\beta}}{\max\left(\alpha_{max} - \alpha_p, \epsilon(1 - \alpha_p)\right)} \tag{10}$$

Here, α_p is the volume fraction of the particle phase, and α_{max} is the packing limit. A small value ϵ is used to ensure numerical stability as α_p approaches or exceeds the limit. The values used in the present work are $P_s = 10$, $\beta = 2$, $\alpha_{max} = 0.65$ and $\epsilon = 10^{-7}$. The interphase force between particles and fluid (gas and liquid mixture) per unit volume is computed as

$$\boldsymbol{F} = \int\int\int f \rho_p \Omega_p \left(D_p(\boldsymbol{U} - \boldsymbol{U}_p) + \frac{\rho}{\rho_p}\left[\frac{D\boldsymbol{U}}{Dt}\right]_p - g\ \frac{\rho}{\rho_p}\right) d\boldsymbol{U}_p d\rho_p d\Omega_p \tag{11}$$

It is worth noting that in addition to the drag and pressure gradient considered in this work, other forces such as lift and virtual mass can be included. The MP-PIC method allows tracking a number particles in a computational parcel as mentioned above. Recently, Kim et al. (2020) solved a homogeneous population balance equation (PBE) for each parcel. In the present work, one computational parcel represents a single particle, and its size is constant. The relation between the particle volume fraction α_p and the probability distribution function f is as follows:

$$\alpha_p = \int\int\int f \Omega_p d\boldsymbol{U}_p d\rho_p d\Omega_p \tag{12}$$

In the coupled MP-PIC and VOF framework there is a contradiction regarding the mesh resolution. It is known that the stability and accuracy of the MP-PIC simulation is dependent on the size ratio between parcels and cells. Since the

interaction between particles as well as phases is described on the basis of mean properties on the Eulerian mesh, it is desirable to have many parcels in a cell to enhance the accuracy of averaged particle effects, which implies that the size of parcels should be several times smaller than the cell size. On the other hand, the solution of governing equations for the fluid phase requires a fine mesh in order to capture the liquid velocity, bubble shape and rise velocity as well as the gas-liquid interface accurately. To overcome this limitation, Caliskan and Miskovic (2021) proposed a chimera approach, which uses two overlapping meshes in the Lagrangian-Eulerian framework - a fine mesh for the CFD fields and a coarser mesh for the MP-PIC fields. The first use of overlapping grids was reported by Volkov (1968), and then further developed and promoted by different Scholars for example for complex geometries and CFD applications. Since 2010's most commercial CFD solvers and many open-source codes use it with structured and unstructured meshes. The recent version of OpenFOAM supports it as well. In the present work, it is implemented in the MPPICInterFoam solver and applied for the investigation of particle effects on bubble coalescence. The modified solver is referred to as chimMPPICInterFoam . For more details about the approach the reader is referred to the original reference.

3. Validation of the method

The coupled method and solver presented above is validated for three specific cases: a) single bubble rising in stagnant liquid, b) single particle setting in pool, and c) bubble pair coalescing in slurry. Experimental data and predictions of other solvers from the literature are used for comparison, and the dependency of numerical results on mesh resolution is investigated in detail.

3.1. Free rising of single bubble in pool

To prove that the chimMPPICInterFoam solver is equivalent to interFOAM for gas-liquid two-phase flow, free rising of single bubble in pure liquid is simulated. The reference case is setup according to the experimental and numerical study of Raymond and Rosant (2000) and Albadawi et al. (2013). The physical properties and parameters used for the simulations are summarized in Table 1. The simulations are two-dimensional and the domain is uniformly discretized. The initially spherical and stationary bubble is accelerated quickly and rises up due to buoyancy. The

μ_l [Pa·s]	ρ_l [kg/m^3]	μ_g [Pa·s]	ρ_g [kg/m^3]	σ [N/m]	g [m/s^2]	d_b [mm]
0.7	1250	1.82×10^{-5}	1, 205	0, 063	9.1125	5

Table 1: Physical properties and simulation parameters for bubble rise simulation

change of bubble velocity with time is shown in Figure 1(a), from which one can see that the acceleration is complished within 50 milliseconds. From $t = 0.1$ s on, the bubble rises steadily at a velocity around 3.3 cm/s. The predictions of chimMPPICInterFoam and interFoam are almost identical, and both conform with the measured terminal rise velocity.

The mesh-independency study shows that if the mesh is finer than $25d_b$, which means that $d_b/\Delta x \geq 25$ with Δx as cell size, the predicted bubble velocity can be considered as mesh-independent, see Figure 1(b). Furthermore, the bubble shape remains nearly spherical as it rises through the liquid medium, which is consistent with the experimental observation of Raymond and Rosant (2000) and numerical results of Albadawi et al. (2013) obtained with a coupled VOF and LS (Level-Set) method.

3.2. Settling of single particle in pool

The setting of single particle in stagnant water pool is simulated to validate the effectiveness of the MP-PIC method and chimMPPICInterFoam solver. The data for setting up the case and validation of the results are taken from the work of Jing et al. (2016). Main parameters are listed in Table 2. The two-dimensional computational domain is 300 mm and

μ_l [Pa·s]	ρ_l [kg/m^3]	ρ_p [kg/m^3]	g [m/s^2]	d_p [mm]
9.98×10^{-4}	998.2	1500	9.81	0.5

Table 2: Physical properties and simulation parameters for particle settling simulation

800 mm high, and the mesh size is uniform in both directions. The particle is initially located at a height of 700 mm and

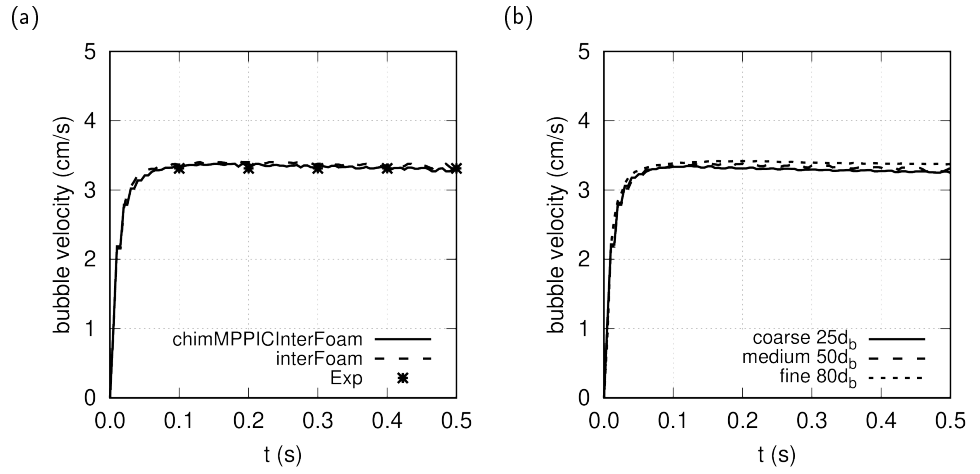

Figure 1: Validation of the coupled solver for single bubble rising (a) against interFoam and experiment (Raymond and Rosant, 2000) (b) mesh-independency study

horizontally in the middle. Similar to the bubble rising case discussed above, the particle settles and accelerates from $t = 0$ s under the effect of gravity. A steady settling velocity is reached when the drag is sufficient to counteract with the gravity. Figure 2 (a) shows the comparison of particle velocity predicted by chimMPPICInterFoam with results of the Wen and Yu correlation (Wen, 1966) and the Jing et al. (2016). The Wen & Yu correlation data were obtained by solving the equation of motion for a single particle assuming drag is only interaction force between the particle and liquid, while the latter was obtained with a CFD-DEM (discrete element method)-VOF coupled solver (cfdemSolverVOF). As one can see that the results of chimMPPICInterFOAM solver are identical to that of the Wen & Yu correlation, which indicates that the combined correlation of Ergun (1952) and Wen (1966) used in chimMPPICInterFoam is similar to the original correlation of Wen (1966) for this case. On the other hand, the prediction of Jing et al. (2016) using cfdemSolverVOF is obviously lower.

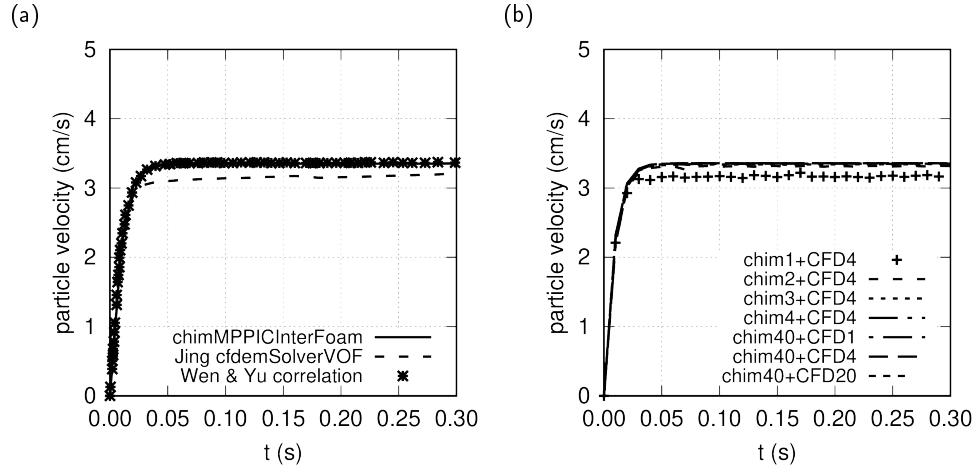

Figure 2: Validation of the chimMPPICInterFoam solver for single particle settling in water (a) compared with theoretical and reference results (b) mesh independency study

The mesh study is plotted in Figure 2 (b) for different chimera and CFD mesh resolutions, where "CFD4" and "chim4" implies that the mesh size for CFD fields (in this case water) and the MP-PIC fields is 4 times of the particle size, respectively. One can see that for this case the CFD mesh resolution has negligible effect on the particle velocity,

which is understandable since the settling of a single particle hardly influences the pool hydrodynamics and the liquid remains nearly stationary. On the other hand, if the chimera mesh size is comparable to the particle size, the settling velocity tends to be under-predicted, and the difference vanishes if it is larger than 4 times particle size. Therefore, in the following studies on bubble coalescence, a ratio of 5 is used.

3.3. Coalescence of a bubble pair in slurry

Finally, the rising and coalescence of a bubble pair in slurry is simulated with chimMPPICInterFoam, and its effectiveness is validated with the CFD-VOF-DPM (discrete phase model) simulations of Liu and Luo (2018). The simulation domain has dimensions of 30 mm width and 80 mm length, and is discretized into a number of square cells. The cell size for the CFD fields is 0.2 mm, which is the same as in the reference, and the MP-PIC mesh size is $5d_p$, i.e. 0.5 mm. At $t = 0$ s the domain is filled with liquid, 1000 particles distributed randomly inside it, and two 10 mm bubbles are positioned co-axially in lower part of the domain. The initial distance between the centres of the two bubbles is 2 or 2.5 times of bubble diameter. A summary of physical properties, bubble and particle diameters is given in Table 3. Note that the particle diameter is reduced to 0.1 mm in the present study, since a too large particle, e.g. $d_p \geq 0.5mm$, leads to high spurious currents at the beginning of the simulation and thereby destroys the gas-liquid interface in this case. The sequence of snapshots in Figure 3 show the rising, approaching and coalescing process of

μ_l [Pa·s]	ρ_l [kg/m^3]	μ_g [Pa·s]	ρ_g [kg/m^3]	ρ_p [kg/m^3]	σ [N/m]	d_p [mm]	d_b [mm]
0.0529	1206	1.8×10^{-5}	1.1	2500	0.0629	1.0(0.1)	10

Table 3: Physical properties and simulation parameters for bubble coalescence

the two bubbles. The upper row of pcitures are results of this work, and the below ones are from the literature. They are in a qualitatively good agreement. As one can see, the bubbles deform substaintially during their rising due to

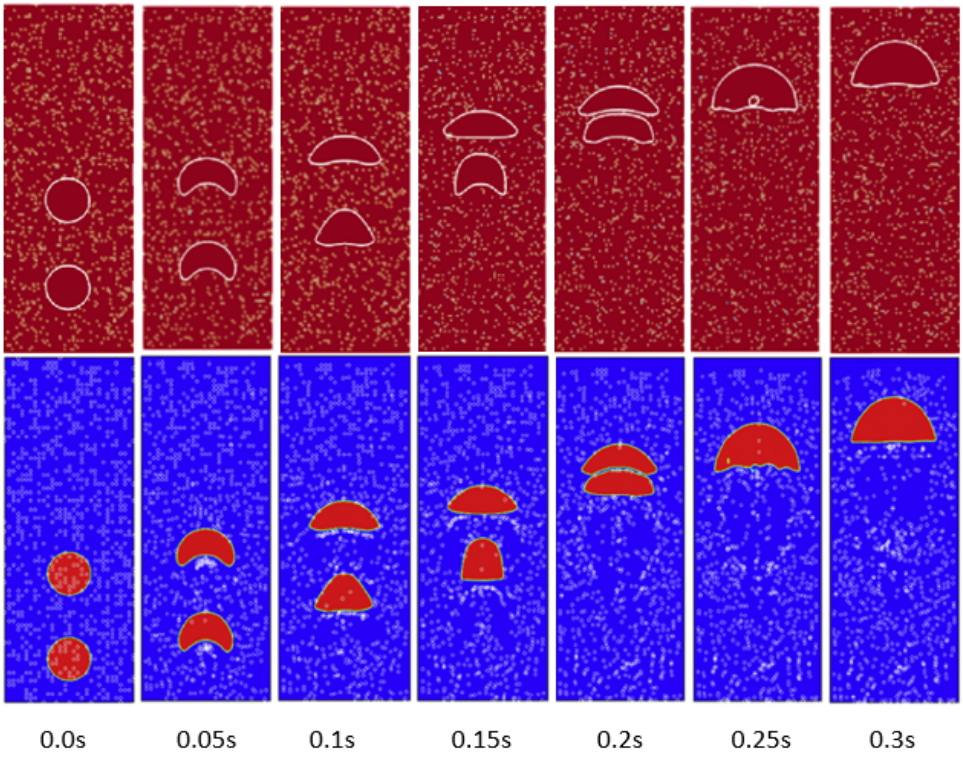

Figure 3: Validation of the chimMPPICInterFoam solver for bubble-pair coalescence in slurry – snapshots. Up: this work, Down: CFD-VOF-DPM simulation results of Liu and Luo (2018)

pressure difference along the interface. At $t = 0.05$ s, because the pressure at the bottom is larger than that at the top, the bubble is dented from below, which gives rise to a wake region behind them. Afterwards the leading bubble evolves rapidly to a cap shape, but the trailing bubble elongates more significantly in the vertical direction due to the wake effect. Its bottom is firstly flattened and then concaved again as it approaches the leading bubble, see $t = 0.10$ s and $t = 0.15$ s. It is accelerated in the wake region and catches up with the leading bubble in about 0.2 s and is flatten in the horizontal direction. After a short interaction and film drainage stage, the two bubbles finally coalesce forming a large cap bubble. The moment at which they coalesce agree well between the two sets of simulations. Nevertheless, slight difference exists in the prediction on bubble shape, e.g. for the trailing bubble at $t = 0.15$ s. According to the CFD-VOF-DPM simulation of Liu and Luo (2018) its bottom is still nearly flat like at $t = 0.1$ s, while the present study shows that it begins to concave again like at $t = 0.05$ s. It implies that at this moment in time, the velocity of trailing bubble predicted by chimMPPICInterFoam is larger than by the CFD-VOF-DPM solver. The distance between two bubbles confirms this speculation, which is shorter in the present simulation. Furthermore, the reference picture shows more significant movement of particles driven by the bubble wake. The deviation might be caused by the reduction of particle size in addition to the methodological difference. Nevertheless, the chimMPPICInterFoam simulations with $d_p = 0.1$ mm and $d_p = 0.2$ mm deliver almost identical results.

Figure 4 shows further the velocity versus time curve for two cases, one with an initial distance H_{ini} of $2d_b$ and the other with $H_{ini} = 2.5d_b$. One can see that the changing course of the leading and trailing bubbles is similar in

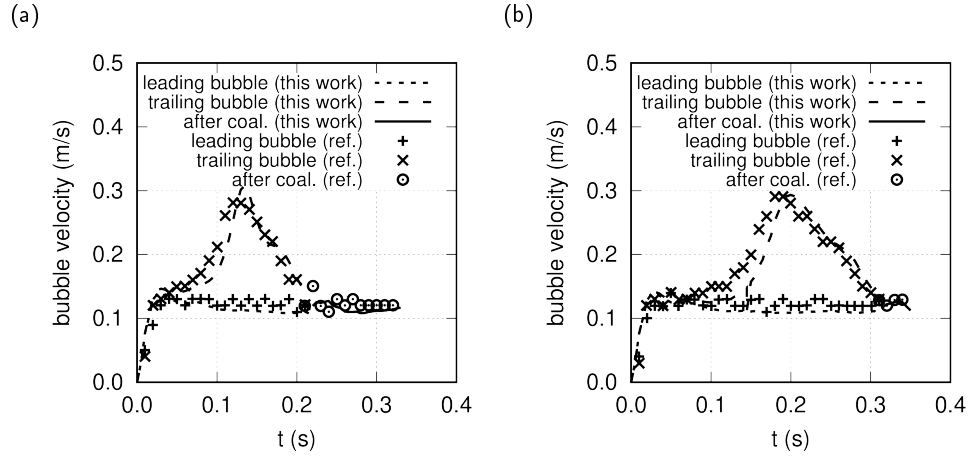

Figure 4: Validation of the chimMPPICInterFoam solver for bubble-pair coalescence in slurry – velocity. (a)initial distance between the bubbles is $2d_b$ (b)initial distance between the bubbles is $2.5d_b$

two cases. The acceleration of the leading bubble is accomplished within 0.02 s and afterwards it rises stably with a terminal velocity around 0.12 m/s. The second acceleration stage of the trailing bubble due to the wake effect is substantial, which starts at about $t = 0.05$ s in the former case while close to $t = 0.1$ s in the latter one. Compared to the reference results, the trailing bubble is accelerated more slowly, but the maximum velocity around $t = 0.15$ s is higher in the case of $H_{ini} = 2d_b$. Apart from that, the predictions of chimMPPICInterFoam and CFD-VOF-DPM solver are in conformity with each other in the respects of the leading bubble, the deceleration stage of the trailing bubble as it approaches the leading one, the coalescence time as well as after the coalescence.

4. Particle effects on bubble coalescence

Based on the last validation case, particle effects on bubble coalescence is investigated in more detail. At first, the influence of domain size is studided by performing simulations in three domains with different widths, i.e. $W/d_1 = 8$, 6 and 3, where W and d_1 represents the domain width and the leading bubble diameter, respectively. It is found that when the ratio is too small, the deformation of bubbles is confined obviously in the direction of domain width, see Figure 5. As W/d_1 increases from 3 to 6 the maximal extension of bubbles in the horizontal direction increases accordingly, which even leads to breakup of the trailing bubble at $t = 0.2$ s. The results show that whether there are wall

effects depends not only on the initial bubble size but also on its final deformation. The conclusion of Mukundakrishnan et al. (2007) that when $W/d_1 \geq 3$, the effect of sidewalls is minimal, is not valid in the present study. In order to avoid the breakup of bubbles during the coalescence caused by wall effects, the size of trailing bubble d_2 is reduced to 7.5 mm. As shown in Figure 6, both bubbles remain intact during the deformation up to coalescence, and the results in $W/d_1 = 8$ and $W/d_1 = 6$ domains are almost identical. The simulations presented in the following are all carried out in a domain with a width of 60 mm and a height of 100 mm, satisfying $W/d_1 = 6$, if $d_1 = 10$ mm.

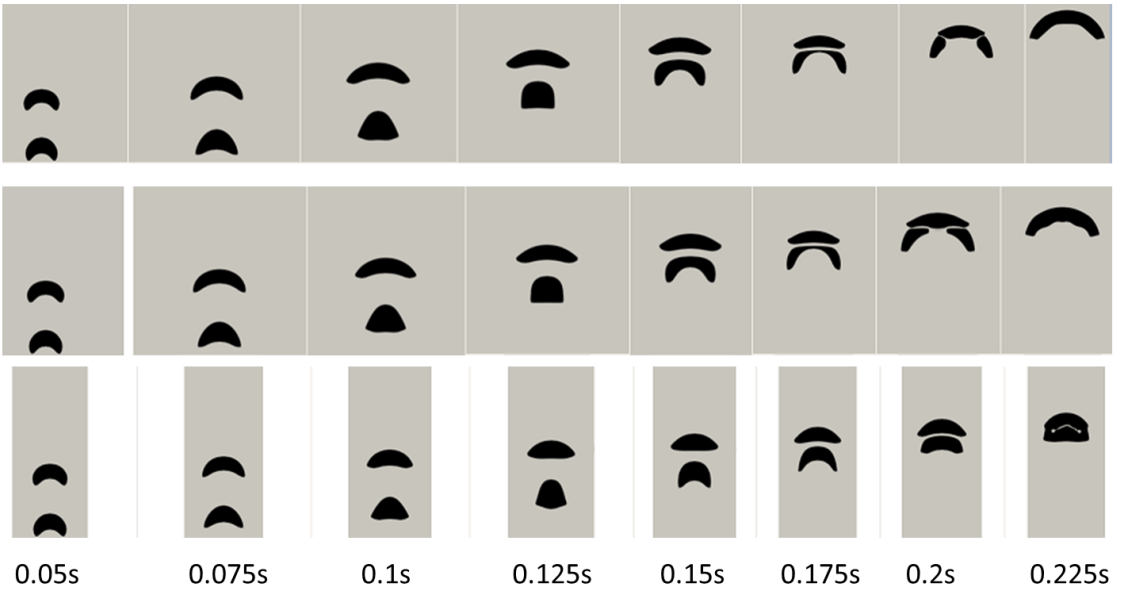

Figure 5: Wall effect on coalescence of a co-axial bubble pair of $d_1 = 10$ mm and $d_2 = 10$ mm. Top: $W/d_1 = 8$, Middle: $W/d_1 = 6$, Bottom: $W/d_1 = 3$

Figure 6: Wall effect on coalescence of a co-axial bubble pair of $d_1 = 10$ mm and $d_2 = 7.5$ mm. Top: $W/d_1 = 8$, Middle: $W/d_1 = 6$, Bottom : $W/d_1 = 3$

4.1. Test cases

Altogehter 17 cases are designed to investigate the effect of particle number, size and density as well as the initial position of the bubbles on their coalescence, see Table 4. The cases "coaxial_", "coradial_" and "diagonal_" denote that the two bubbles are positioned initially co-axially, co-radially and diagonally, while d_1, d_2, h_h, h_v, N_p, d_p, ρ_p represent the diameter of leading and trailing bubble, initial distance in the horizontal and vertical direction, number, diameter and density of particles, repsectively. In the co-axial cases, six particle numbers, three particle diameters and densitites are compared. The gas and liquid properties are kept constant, i.e. $\rho_l = 1206$ kg$\cdot$ m^{-3}, $\rho_g = 1.1$ kg$\cdot$ m^{-3}, $\mu_l = 0.529$ Pa$\cdot$ s, $\mu_g = 1.8\times10^{-5}$ Pa$\cdot$ s, $\sigma = 0.0629$ N/m. In addition, the particles are assumed insoluble hydrophilic, and their influence on the gas-liquid interface properties is ignored.

case	d_1 [mm]	d_2 [mm]	h_h [mm]	h_v [mm]	N_p [-]	d_p [mm]	ρ_p [kg $\cdot$ m^{-3}]
coaxial_0	10	7.5	0	17.5	0	0.1	2500
coaxial_1	10	7.5	0	17.5	10^4	0.1	2500
coaxial_2	10	7.5	0	17.5	8×10^4	0.1	2500
coaxial_3	10	7.5	0	17.5	10^5	0.1	2500
coaxial_4	10	7.5	0	17.5	2×10^5	0.1	2500
coaxial_5	10	7.5	0	17.5	4×10^5	0.1	2500
coaxial_6	10	7.5	0	17.5	10^4	0.2	2500
coaxial_7	10	7.5	0	17.5	10^4	0.05	2500
coaxial_8	10	7.5	0	17.5	8×10^4	0.1	1250
coaxial_9	10	7.5	0	17.5	8×10^4	0.1	5000
coaxial_10	10	7.5	0	17.5	4×10^5	0.1	1250
coaxial_11	10	7.5	0	17.5	4×10^5	0.1	5000
coaxial_12	10	7.5	0	17.5	1.6×10^6	0.05	2500
coaxial_13	10	7.5	0	17.5	1.8×10^5	0.15	2500
coaxial_14	7.5	7.5	0	15	8×10^4	0.1	2500
diagonal_1	7.5	7.5	7.5	7.5	8×10^4	0.1	2500
coradial_1	7.5	7.5	8.5	0	8×10^4	0.1	2500

Table 4: Overview of investigated cases

4.2. Effect of mesh size

The study of bubble coalescence requires a high spatial resolution, since the film drainage process which governs the rate of coalescence usually takes place at a length scale ranging from millimeter to nanometer. For example, for air-water systems Prince and Blanch (1990) assumes that the drainage starts at an initial film thickness of 10^{-4} m, and ceases at the thickness of 10^{-8} m, when the van der Waals force becomes dominant and a hole is rapidly formed leading to coalescence. Available references such as Kim and Lee (1987); Kirkpatrick and Lockett (1974); MacKay and Mason (1963); Marrucci (1969); Scheludko et al. (1965); Vrij (1966) support these assumptions on the initial and critical film thickness. However, because the computational load increases with the number of cells dramatically, most numerical studies with interface capturing approaches have a resolution less than (or cell size larger than) 0.1 mm, e.g. $\Delta x = 0.2$ mm chosen in Liu et al. (2014) and Liu and Luo (2018). Chakraborty et al. (2013) and Mukundakrishnan et al. (2007) suggested a ratio of 0.02 and 0.01 for mesh to bubble sizes, respectively, which means that for 10 mm bubbles $\Delta x = 0.2$ mm and $\Delta x = 0.1$ mm can be used. Feng et al. (2016) adopted a grid size of 0.05 mm for their VOF study on coalescence of two in-line bubbles at low Reynolds numbers. In the present work, the minimum cell size is down to 0.05 mm to show its effect on bubble approach velocity, film drainage mechanism as well as particle effect. Figure 7 shows the results for case coaixal_0 in Table 4. From left to right the mesh size decreases from 0.4 mm to 0.05 mm. As one can see, the difference appears first after $t = 0.16$ s, in other words, when the two bubbles are close enough to each other. If the mesh is too coarse, e.g. $\Delta x = 0.4$ mm, artificial breakup of the trailing bubble prior to the coalescence is observed. Naturally, the bubbles come to merge and coalesce later as the mesh is refined, for example, at $t = 0.19$ s with $\Delta x = 0.2$ mm and $t = 0.25$ s with $\Delta x = 0.05$ mm. Thus, it is impossible to get mesh-independent results for the onset of coalescence. Nevertheless, the difference in bubble deformation and shape change during the

coalescence for $\Delta x = 0.1$ mm and $\Delta x = 0.05$ mm is minimal, and the latter is already in the film drainage range. To reduce the computational cost, the mesh size of 0.05 mm is adopted to investigate particle effects on the film drainage process further.

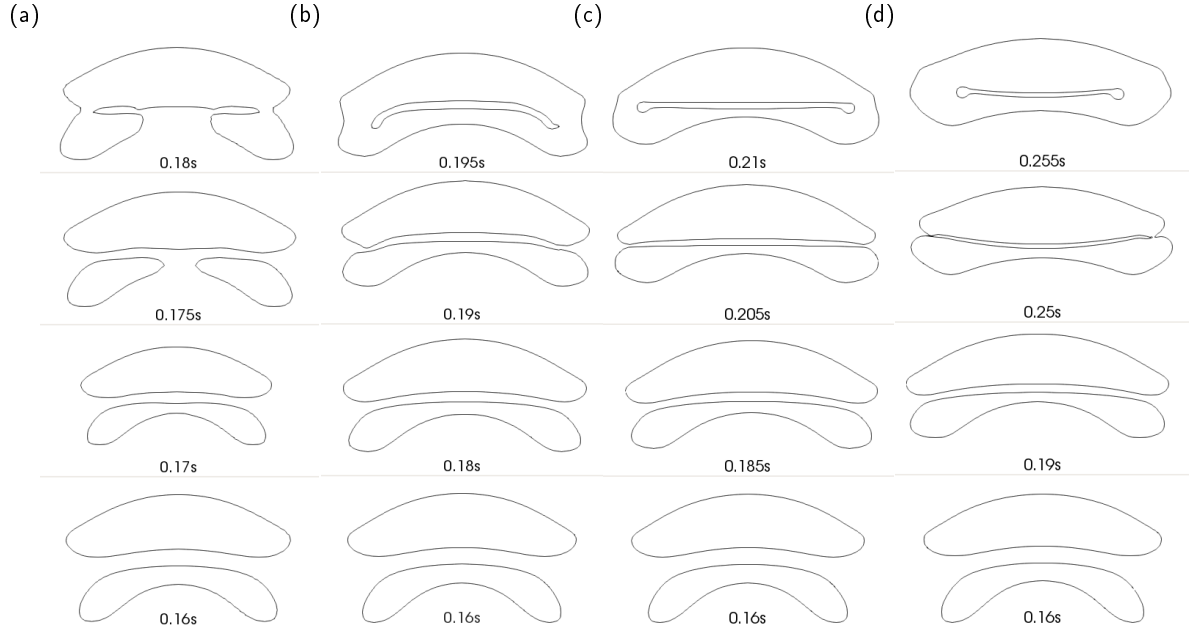

Figure 7: Effect of CFD cell size on the coalescence behavior in case coaixal_0, (a) $\Delta x = 0.4$ mm, (b) $\Delta x = 0.2$ mm, (c) $\Delta x = 0.1$ mm, (d) $\Delta x = 0.05$ mm

4.3. Effect of particle number

The coalescence behavior of two co-axial bubbles is investigated first by increasing the number of particles distributed on the plane of interest while keeping other parameters such as the size of bubbles and particles unchanged (see the cases coaxial_0 ∼ coaxial_6 in Table 4). It is worth mentioning that for $N_p \geq 10^5$ the initial distribution of particles changes from random to uniform in order to increase the maximum packing limit, and the intersection between particles is avoided intentionally in all cases. Figure 8 shows that the presence of particles has little influence if the number concentration is sufficiently low, say $N_p < 10^5$, which corresponds to an area ratio around 13.1% of the 2D simulation plane occupied by particles. In all the pictures solid white lines are contours of liquid volume fraction equal to 0.5 representing the shape of bubbles, the grey points denote particles while the color of the display plane is scaled with the velocity magnitude between 0 and 0.5 m/s. In cases coaxial_0 and coaxial_1, the bubbles approach to each other axisymmetrically up to the occurrence of coalescence. The rising of bubbles gives rise to a high-velocity wake region, which is the reason why the smaller trailing bubble is able to catch the leading one and eventually coalesce with it. Furthermore, the deformation of bubbles generates non-uniform velocity distribution inside them with high values in the stretched parts. At low particle concentrations, the liquid between the interacting interfaces drains out approximately uniformly from both sides. In other words, the film thins evenly, and the majority of particles are pushed away from the film without direct influence on the coalescence. The same scenario happened in the experimental studies of Spyridopoulos et al. (2004) and Omota et al. (2005) in a coalescence cell with two vertical needles in opposite directions, i.e. co-axial collision, and one or several hydrophilic particles being placed between the two approaching bubbles. The deformation and coalescence dynamics is similar to that in pure liquid ($N_p = 0$). The two bubbles remain aligned co-axially, and the colliding interfaces is first flattened and then dimpled during the drainage. The smallest film thickness is located at the rim of the dimple, which ruptures first leading to coalescence. As the number of particles exceeds 8×10^4, the drainage and thinning of liquid film becomes asymmetrical and coalescence of bubbles starts at one side, see cases coaxial_2 and coaxial_3. The degree of asymmetry seems to increase with the particle concentraion, and consequently the one-side coalescence occurs earlier, which is supposed to be a reason

for enhanced coalescecnce rate by particles. However, if N_p increases further, e.g. $N_p = 2 \times 10^5$, the coalescence is significantly retarded because of the obstructing effect of particles present in the film, and bubbles begin to slide and rotate about the interacting interface. For example, in the first four cases with $N_p \leq 10^5$ coalescence occurs approximately around $t = 0.25$ s, where in case coaxial_4 the film ruptures first at $t = 0.28$ s. It is interesting to observe that the coalescence is advanced again in coaxial_5, which happens at $t = 0.271$ s. Note that a similar dual effect with respect to solid concentration C_s has been reported by Khare and Joshi (1990) and Rabha et al. (2013b). The latter measured the bubble size and radial gas hold-pp distribution in a 3D slurry bubble column with ultrafast electron beam X-ray tomography. They found that if C_s larger than 0.05 bubble coalescence is significantly promoted, but larger than 0.2 the bubble size tends to decrease again. The scholars attributed this result to possible breakup events, while this study reveals that the change of coalescence behavior may alone lead to such dual effects. The mechanism of interface collapse and coalescence is supposed to be different in the low and high concentration regimes. In the former, contact of the interfaces occurs at the location where the film thickness is the smallest and no particle obstruction exists, while in latter, the destroying of liquid film and interface stability is caused by the particles or their motion. As a result, the interfaces stretch more slowly and becomes instable more quickly as the particle concentration increases.

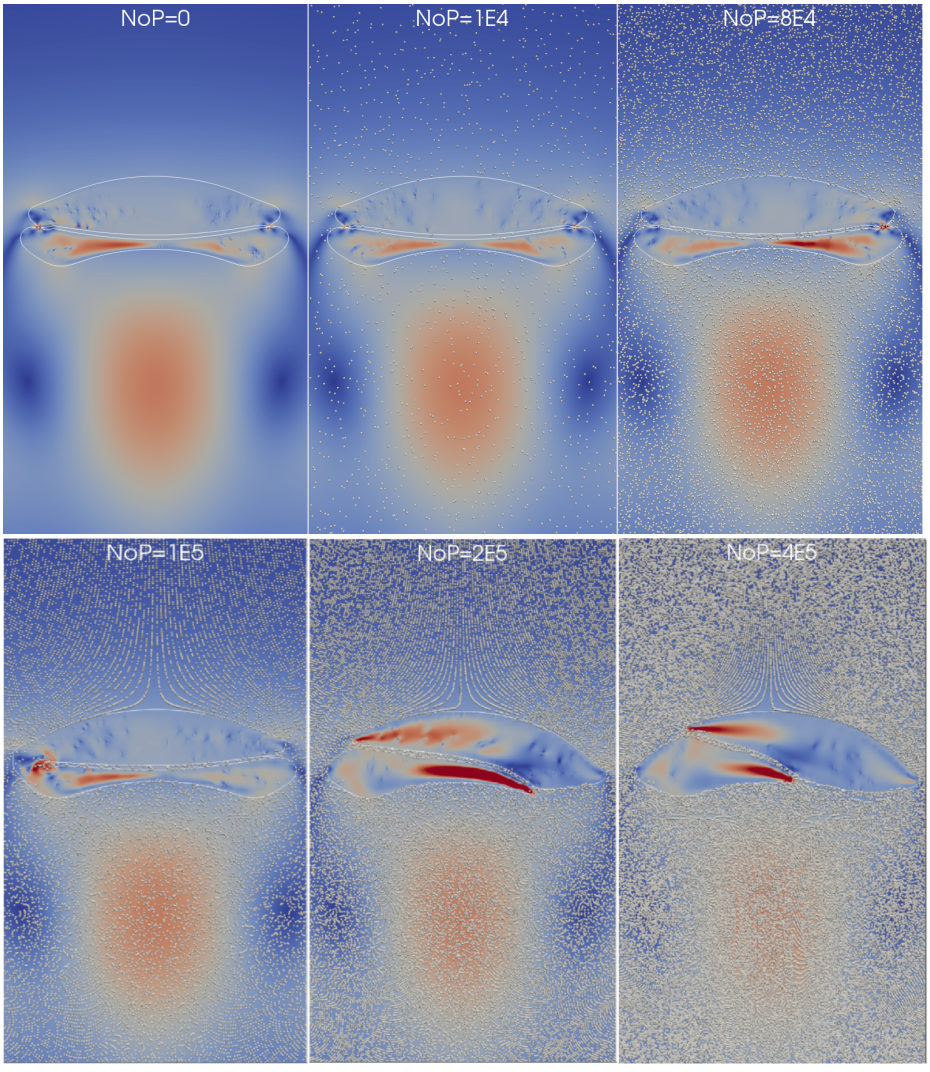

Figure 8: Effect of particle number on film drainage and coalescence behavior at $t = 0.25$ s. From left to right, top to bottom: coaxial_0 ($N_p = 0$), coaxial_1 ($N_p = 10^4$), coaxial_2 ($N_p = 8 \times 10^4$), coaxial_3 ($N_p = 10^5$), coaxial_4 ($N_p = 2 \times 10^5$), coaxial_5 ($N_p = 4 \times 10^5$). Other conditions of the cases are listen in Table 4.

The moment at which film rupturing and coalescence taking place is shown in Figure 9 for cases coaxial_1, coaxial_4 and coaxial_5. In the first case with $N_p = 10^4$, the bubbles remain vertically aligned. Because of relatively large film radius, a dimple is formed at the later stage of drainage and the thinnest liquid film is identified at the rim, which ruptures leading to coalescence finally. The mechanism of dimple formation and dimple drainage has been investigated widely for two-phase systems, e.g. bubbles in pure liquid and droplets in gas (Chan et al., 2011; Liu et al., 2019; Ozan and Jakobsen, 2019). Due to the particle effects, the position of bubbles changes from initially co-axial to side-by-side at the moment of coalescence in the two cases with a higher particle concentration, without forming a dimple. As discussed above, this alignment change is observed at the film drainage stage as the bubbles are close enough to each other, while at the approaching stage, the presence of particles is found to have limited impact in the investigated range, for example on the shape and velocity of bubbles. In addition, in coaxial_4 and coaxial_5 the film thickness is nearly uniform between the two interfaces, which turn to wavy and instable as the film thins to a certain point. Correspondingly, the velocity field of the film flow and in gas boundary layer adjacent to the interfaces becomes non-uniform with local increase in narrow places. Finally, the interfaces collapse leading to coalescence, which starts at the lower part of the film.

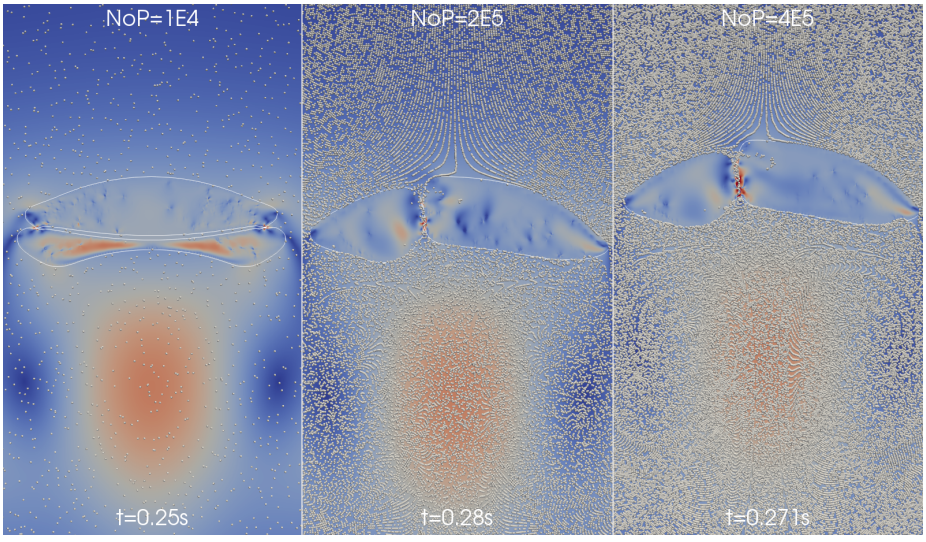

Figure 9: The moment of coalescence in difference cases. From left to right: coaxial_1 ($N_p = 10^4$), coaxial_4 ($N_p = 2\times10^5$), coaxial_5 ($N_p = 4\times10^5$). Other conditions of the cases listen in Table 4.

In order to show how the particle concentration affects the film shape, orientation and drainage during the coalescence process in more detail, the contours of liquid volume fraction equal to 0.5 are depicted for different time points in Figure 10 for the above six cases. As the two spherical bubbles start to rise up, the smallest distance is first located at the middle and the drainage is rapid, even when the leading bubble begins to concave at the bottom, see the pictures of $t = 0.05$, 0.1 and 0.15 s in Figure 3. As the liquid film between the bubbles becomes thin, the rate of thinning is retarded because of increased viscous resistance. As a response, radial pressure gradients arise to remove the interventing film, which leads to the formation of a dimple, e.g. at the time point of 0.19 s in Figure 10. At $t = 0.21$ s the convex dimple is pushed out and a plane parallel film results in all cases. As the drainage proceeds further, the curvature at the center changes its sign and a new concave dimple is formed, see the moment of $t = 0.23$ s. In the first four cases ($N_p = 0$, $N_p = 10^4$, $N_p = 8\times10^4$, $N_p = 10^5$) the dimple remains and the rupture occurs on its surrounding rim. Whereas in the last two cases with $N_p = 2\times10^5$ and $N_p = 4\times10^5$, the dimple is pushed out again and the plane parallel film is recovered. At the same time, its orientation changes from horiontal to vertical. In this case, instability results in film rutpure and coalescence.

4.4. Effect of particle density

The effect of particle density is investigated for two number concentrations. As Figure 11 shows, at $N_p = 8\times10^4$ changing the particle density from 1250 kg$\cdot$ m^{-3} to 5000 kg$\cdot$ m^{-3} has negligible effect on the film drainage and

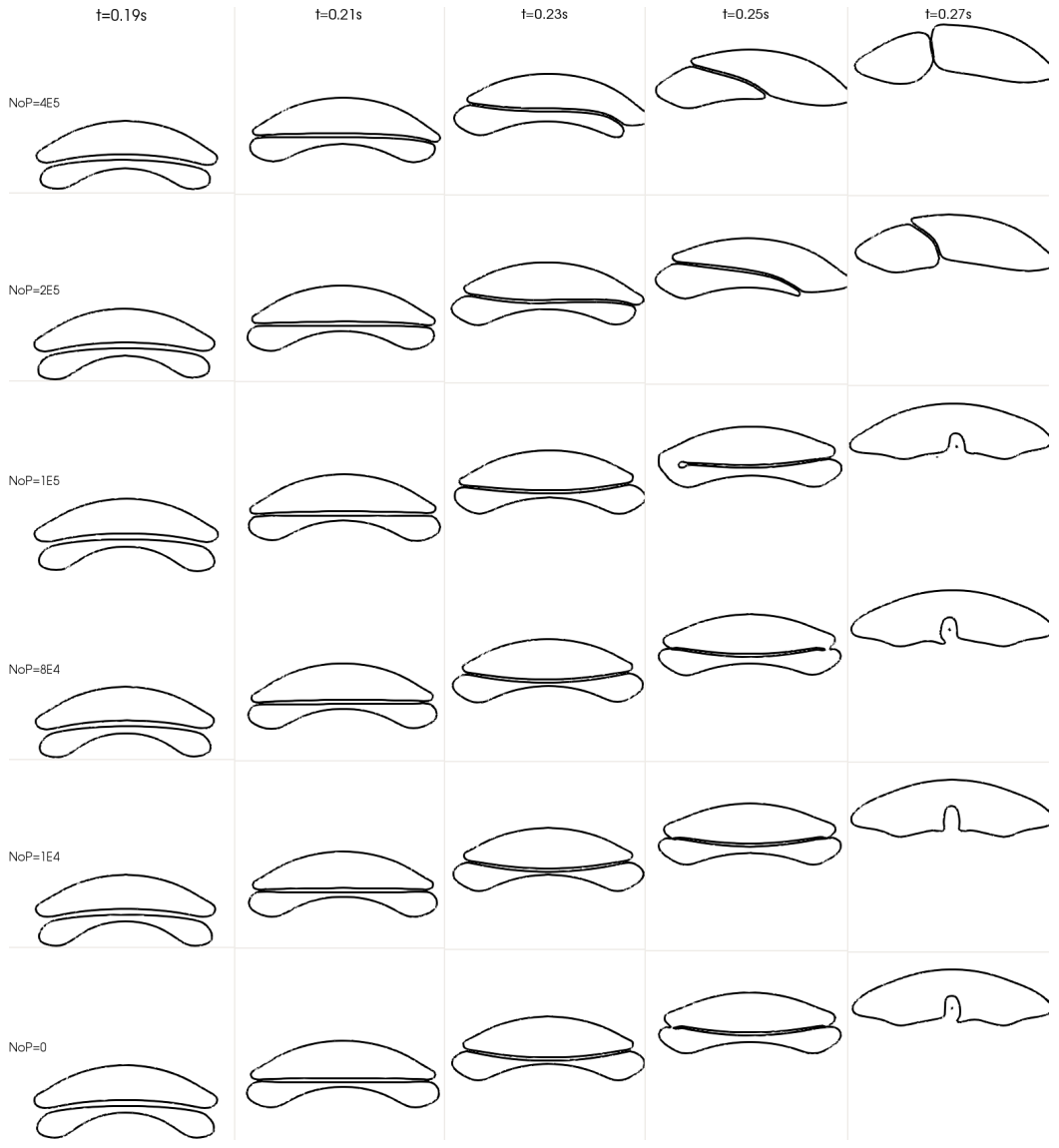

Figure 10: The shape of bubbles and liquid film during the drainage process in difference cases. From bottom to top: coaxial_0 ($N_p = 0$), coaxial_1 ($N_p = 10^4$), coaxial_2 ($N_p = 8 \times 10^4$), coaxial_3 ($N_p = 10^5$), coaxial_4 ($N_p = 2 \times 10^5$), coaxial_5 ($N_p = 4 \times 10^5$). From left to right: $t = 0.19$ s, $t = 0.21$ s, $t = 0.23$ s, $t = 0.25$ s, $t = 0.27$ s. Other conditions of the cases are listen in Table 4.

coalescence dynamics. In all three cases, the interacting interfaces remain nearly horizontal, and the trailing bubble deforms to a dumbbell shape during the film draining and dimple forming stage. As the liquid film ruptures on the rim around $t = 0.25$ s, the lateral streching ceases and the coalesced bubble develops to a cap shape rapidly. At high particle concentrations the orientation of interacting interfaces changes from horizontal to vertical, as the trailing bubble slides from below to the left side of the leanding one, see Figure 12. The particle density has still negligible effect at the film drainage stage. For example, from $t = 0.25$ s to $t = 0.26$ s, the morphology of bubbles is quite similar for the three particle densities. Nevertheless, it is found to have an impact on the film rupture. The film tends to rupture at the lower and upper position successively, and as a result a droplet is enclosed in the coalesced bubble, which will fall out of the lower boundary of the coalesced bubble due to gravity. Increasing the particle density from 2500 kg·m^{-3} to 5000 kg·m^{-3}, the film rupture is advanced. In the case coaxial_5, it occurs at $t = 0.271$ s, while at $t = 0.269$ s in the case

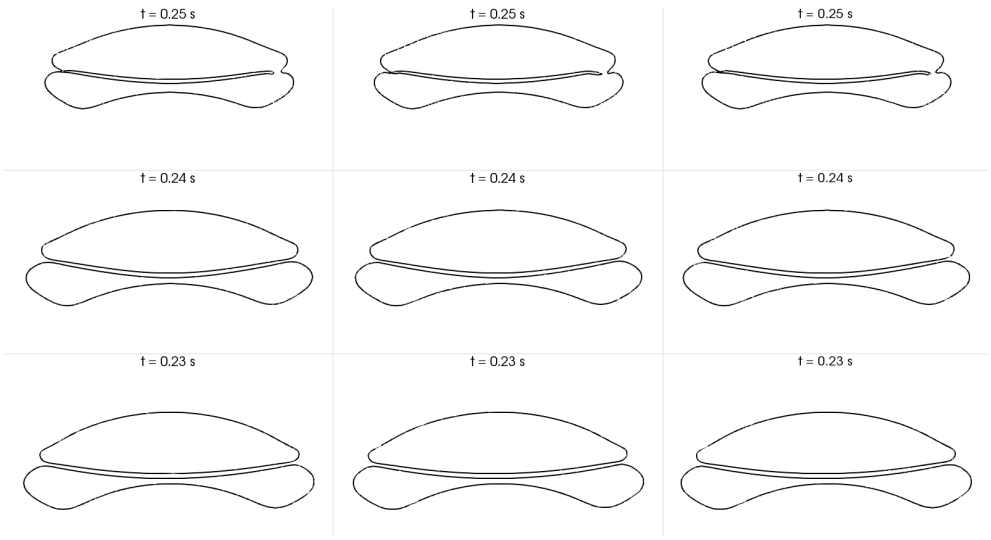

Figure 11: Effect of particle density on film drainage, rupture and bubble deformation at $N_p = 8 \times 10^4$. From left to right: $\rho_p = 1250$ kg·m^{-3} (coaxial_8), $\rho_p = 2500$ kg·m^{-3} (coaxial_2), $\rho_p = 5000$ kg·m^{-3} (coaxial_9). From bottom to top: $t = 0.23$ s, 0.24 s, 0.25 s.

coaxial_11. The effect of particle density on the gas hold-up in three-phase bubble columns has been investigated in Khare and Joshi (1990). They found that alumina particles tend to promote the coalescence of bubbles compared to quartz particles, leading to a decrease of gas hold-up at smaller particles. The main difference is that the former has a density of 4000 kg ·m^{-3}, while the latter 2520 kg ·m^{-3}. It is interesting to observe that the particle density has a dual effect on the film drainage and rupture. In other words, at $\rho_p = 1250$ kg·m^{-3}, which is close to the liquid density, the film ruptures earlier than at $\rho_p = 2500$ kg·m^{-3}. Recall that at high particle concentration the film ruptures as a result of interface instability and film flow jointly. Since there are still a number of particles present in the film, it is understandable that the particle density and relative motion influence its rupture time. Nevertheless, the moving of particles through the vertical film region might be highly complicated. On one side, due to the recirculation in the wake region beneath, the particles tend to rise up with the liquid from the centre, while on the other side, they settle from the top under the effect of gravity. In addition, the narrow cross section of the film prevents them from flowing throught. As a result, a stagnation zone is observed at the lower part of the film, where the rupture first occurs. Whether the rupture at the upper part of the film under high particle density condition results from particle motion needs further studies.

4.5. Effect of particle size

The effect of particle size is first investigated for a constant number of particles, i.e. $N_p = 10^4$. As shown in Figure 13, since the particle number concentration is relatively low, the increase of particle size from $d_p = 0.05$ mm to $d_p = 0.2$ mm has hardly any effect on the film thinning rate and rupture time. At $t = 0.15$ s, 0.2 s and 0.25 s, the bubble shape and film thickness is almost identical, and coalescence starts at about $t = 0.25$ s in all three cases. Nevertheless, a close look reveals that the film ruptures only at one side in coaxial_7 while in other two cases it is observed at both sides. It indicates that if the number is kept constant, increasing of particle size will lead to an increase in the volume (area in 2D) ratio of the particles, which might increase the blocking effect, similar to that observed at higher number concentrations (see cases coaxial_2 and coaxial_3 in Figure 8). It is reasonable to speculate that if the particle size is increased further or at a higher concentration, more substaintial impact on the film drainage like in cases coaxial_4 and coaxial_5 will be observed. Another consideration for investigating the effect of particle size is to keep the area ratio of the 2D plane occupied by the particles constant, which means that the number has to be adjusted while the particle size changes. In the following study, the area ratio of particles is set to 0.524, which is about 3.14×10^3 mm^2, since the simulation plane has an area of 6×10^3 mm^2. Accordingly, there are $N_p = 1.6 \times 10^6$ for $d_p = 0.05$ mm, $N_p = 4 \times 10^5$ for $d_p = 0.1$ mm and $N_p = 1.8 \times 10^5$ for $d_p = 0.15$ mm. They are cases coaxial_12, coaxial_5 and

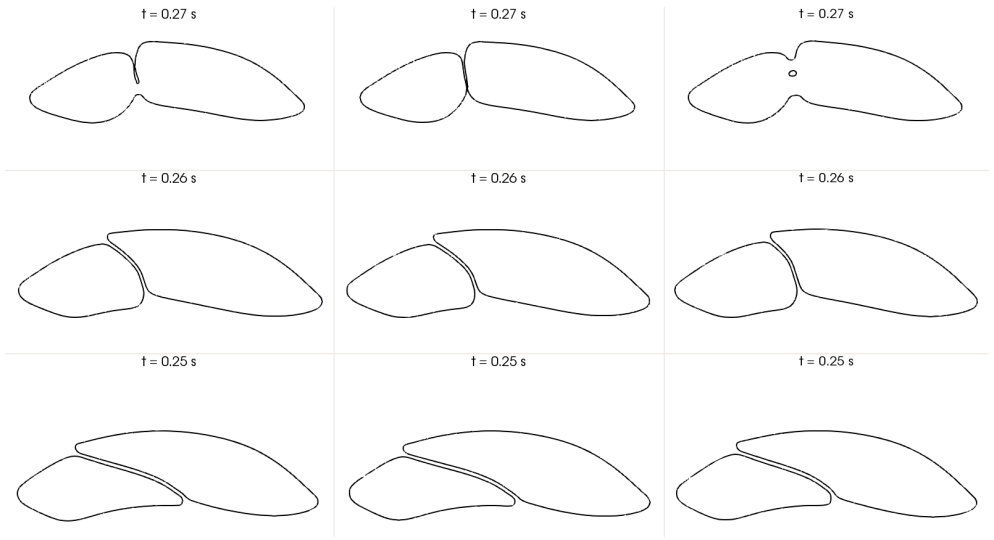

Figure 12: Effect of particle density on film drainage, rupture and bubble deformation at $N_p = 4 \times 10^5$. From left to right: $\rho_p = 1250$ kg· m^{-3} (coaxial_10), $\rho_p = 2500$ kg·m^{-3} (coaxial_5), $\rho_p = 5000$ kg·m^{-3} (coaxial_11). From bottom to top: $t = 0.25$ s, 0.26 s, 0.27 s.

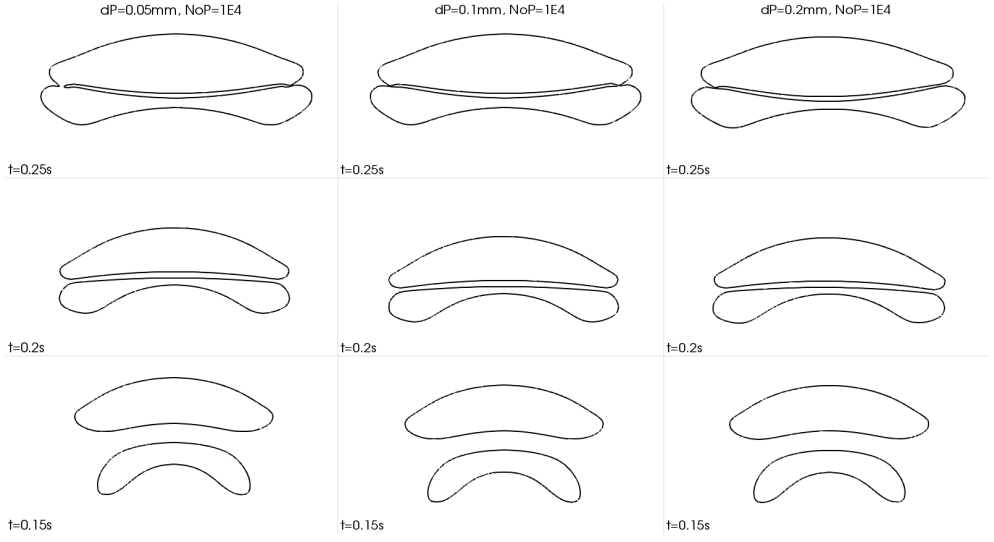

Figure 13: Effect of particle size on bubble coalescence time at $N_p = 10^4$. From left to right: coaxial_1 ($d_p = 0.05$ mm), coaxial_6 ($d_p = 0.1$ mm), coaxial_7 ($d_p = 0.2$ mm).

coaxial_13 in Table 4, respectively. As Figure 14 shows, before $t = 0.2$ s, the bubble pair deforms and approaches similarly, although in case coaxial_13 the vertical position is slightly lower compared to the other two cases. It implies that large particle size may have an impact on the bubble rise velocity during the approaching stage. Furthermore, at $t = 0.2$ s the liquid film between the bubbles seems to become more straight as the particle size increases, which indicates that the convex dimple is pushed out more early. The most significant difference is observed at the moment of coalescence in the apsects of bubble morphology, film rupture position as well as coalescence time, see the top row of pictures in Figure 14. In the case of coaxial_12, the dimple is pushed out at the latter stage of draining but no plane parallel film and concave dimple appear subsequently. The leading bubbles stretches significantly and surrounds the trailing bubble from both sides. A bell-shaped film having nearly uniform thickness forms, which thins further and

ruptures at several locations simultaneously due to instability. In coaxial_5, as discussed above, during the plane film drainage the trailing bubble slides to the left side of the leading one and correspondingly the film orientation changes from horizontal to vertical. The mergence of bubbles occurs first at the lower end of the liquid film and the rupture. As the particle size increases to 0.15 mm and its number decreases to 1.8×10^5, the two bubbles keep vertical alignment during the coalescence. A concave dimple is formed after the plane-parallel stage and the film rupture happens at one side, which is similar to the case coaxial_3 (see Figure 8). The results in Figures 13 and 14 evidence that the effect of particle size is coupled with that of number and/or volume (area) concentration. By investigating bubble size and void fraction distribution in a slurry bubble column under three particle concentrations $C_s(= 0.01,\ 0.03,\ 0.05)$ and sizes $d_p(= 0.05,\ 0.1,\ 0.15)$ mm Rabha et al. (2013a) reported that increasing of both particle size and concentration tends to promote bubble coalescence, and the effect is more significant for $d_p \geq 0.1$ mm and $C_s \geq 0.03$. Khare and Joshi (1990) classified the dependency of gas hold-up in three-phase sparged reactors on particle size and loading into several regimes. At low loading and small particle size gas hold-up increases with the loading, while decreases in other regimes. Both particle size and concentration have a dual effect on the gas hold-up and bubble coalescence probability.

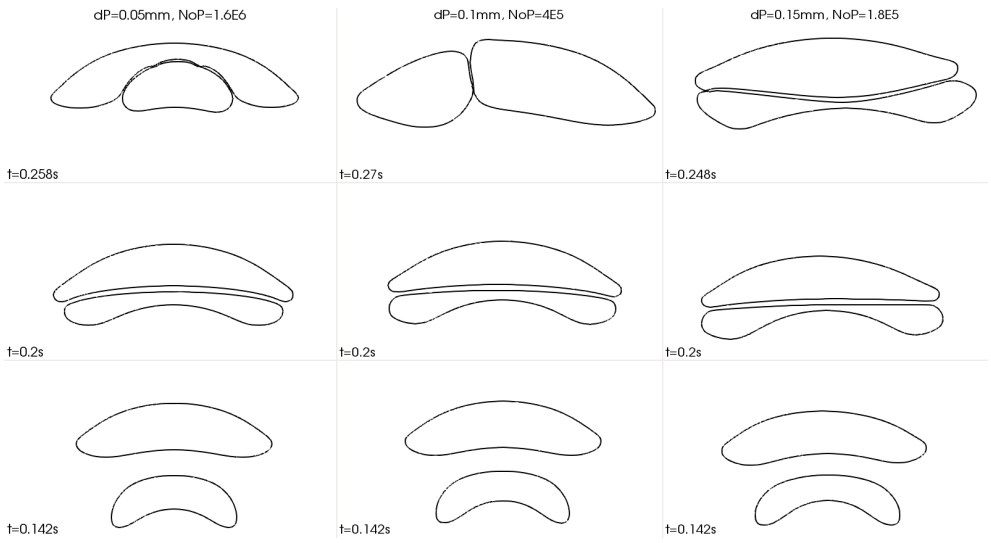

Figure 14: Effect of particle size on bubble coalescence time while keeping the total cross section of particles constant. From left to right: coaxial_12, coaxial_5, coaxial_13.

4.6. Coalescence time

According to Maldarelli and Jain (1988) the coalescence time can be approximated as the duration from the moment in which the relative motion between the bubbles becomes sufficiently low and stable to the rupture of the liquid film. Figure 15 shows the relative rise velocity (defined as the difference of the vertical velocity component of the trailing and leading bubble) in the first six cases, which reflects the influence of particle number concentration. As one can see, the bubbles start to rise up at a similar speed. The velocity difference becomes large as the wake acceleration comes into effect, and decreases again at certain separation. It reaches a flat valley around $t = 0.2$ s, which is considered as the starting moment of film drainage t_d. In the cases coaxial_0, coaxial_1, coaxial_2 and coaxial_3, the drainage processes first under a low but nearly constant relative velocity. After a while, the relative motion is substantially retarded because of large viscous resistance and drops to zero at the moment of film rupture or coalescence occurrence. While in the last two cases, where the number of particles is high, the drainage at constant relative motion does not lead to film rupture but is followed by a sliding motion as discussed above, where the alignment of bubbles changes from vertical to horizontal and the axial relative motion increases again. It is worth mentioning that the film thickness does not increase but continues thinning at a low rate during the sliding. After some delay, film rupture occurs as a result of instability and particle effects. By comparing the case coaxial_5 with coaxial_4, one can see that the starting and duration of the sliding movement is promoted with the increase of particle concentration. In the six co-axial cases, the

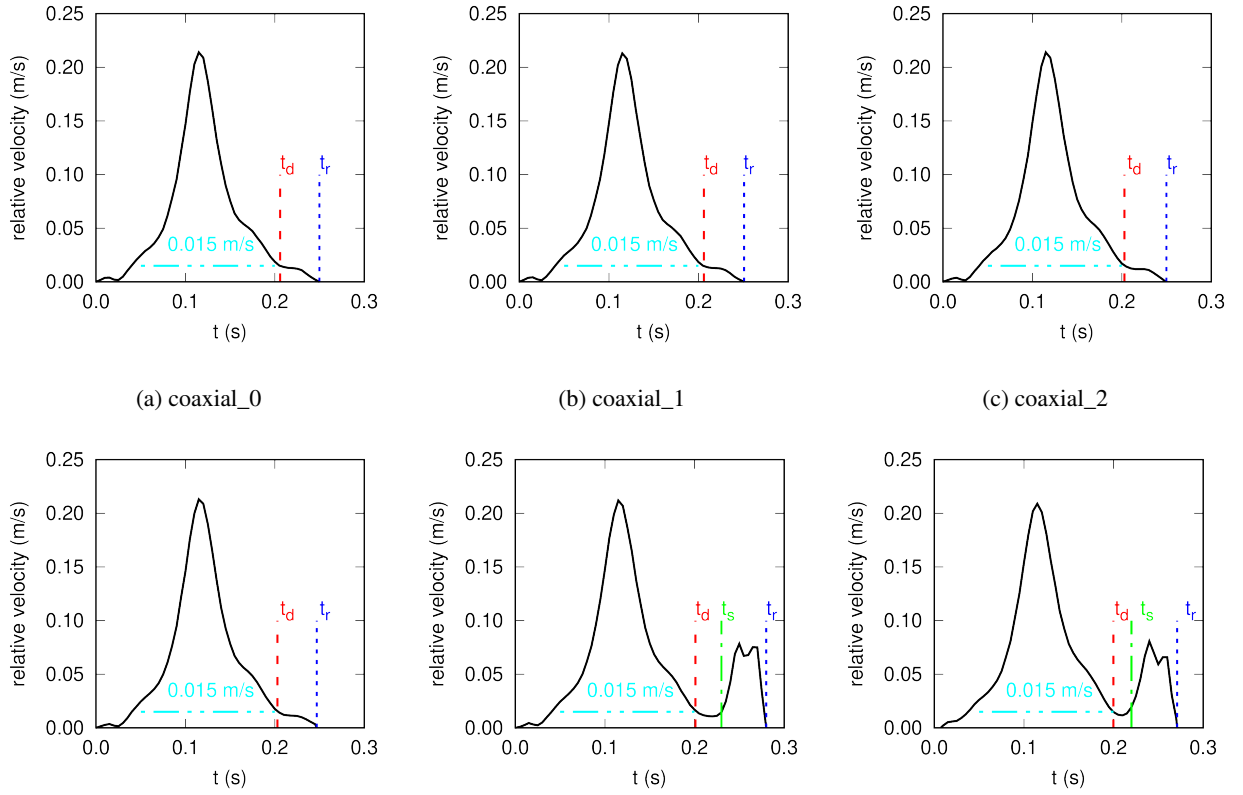

(a) coaxial_0 (b) coaxial_1 (c) coaxial_2

(d) coaxial_3 (e) coaxial_4 (f) coaxial_5

Figure 15: The evolution of relative rise velocity between the two bubbles and the effect of particle number concentrations. The red, blue, green dash and dashdot lines (t_d, t_r, t_s) represent the moment of film drainage starting, film rupture occuring and sliding beginning, respectively.

film drainage valley begins at the condition of a similar vertical relative velocity $U_{rel} = 0.015\ m/s$ as shown in Figure 15. It proves the fact again that the particle number concentration has little influence on the rising and approaching of bubbles, and the impact exists mainly in the drainage stage. As a result, t_d can be quantified with the time point when the axial approach velocity decreases to 0.015 m/s. The results are presented in Table 5, where t_r denotes the time moment of film rupture, and the coalescence time is computed from $t_c = t_r - t_d$. As one can see, the influence of particle number concentration on coalescence time is multimodal, see also Figure 16a. From coaxial_0 to coaxial_2, the presence of particles are shown to have a blocking effect and retard the film drainage and bubble coalescence, and the obstruction increases with the number concentration. The coalescence time is reduced in case coaxial_3 compared to case coaxial_2, because the axisymmetry of drainage is destroyed and one-side rupture/coalescence happens. As the number of particles increases further, the bubbles begin to slide about each other leading to a noticeable increase in the coalescence time. But in case coaxial_5, the occurrence of coalescence is advanced again, which is supposed to be caused by the fact that particle effects on the stability of thin liquid film become significant. Similarly, the effect of particle size and density on the film drainage rate and coalescence time can be evaluated. As shown in Figures 16b and 16c, both the size and density have a dual effect. In other words, increasing of particle size (if the area or volume concentration kept constant) or density tends to first hinder and then promote the coalescence. It is worth noting that Rabha et al. (2013a) measured an enhancement of the coalescence as they increased the particle size from 0.1 mm to 0.15 mm. Similar dual effect on the particle size has been aslo observed by Kim et al. (1987). Compared to the size, the influence of particle density is modest. The multimodal or dual effect of particles on bubble coalescence may explain partially some contradictory reports on experimental findings found in the literature.

case	t_d [s]	t_r [s]	t_c [s]
coaxial_0	0.206	0.25	0.044
coaxial_1	0.206	0.25	0.046
coaxial_2	0.205	0.251	0.047
coaxial_3	0.203	0.25	0.044
coaxial_4	0.201	0.28	0.079
coaxial_5	0.20	0.271	0.071

Table 5: Influence of particle number concentration on coalescence time

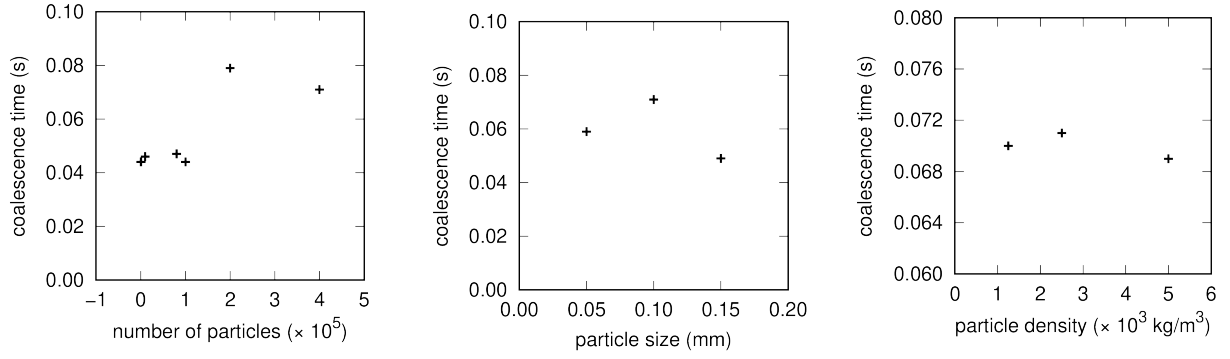

(a) effect of N_p (b) effect of d_p (c) effect of ρ_p

Figure 16: Dependence of coalescence time on number, size and density of particles. (a) effect of N_p: coaxial_0 ∼ coaxial_5; (b) effect of d_p: coaxial_12, coaxial_5, coaxial_13; (c) effect of ρ_p: coaxial_10, coaxial_5, coaxial_11.

4.7. Effect of initial position of bubbles

Finally, the rising of an equal-sized bubble-pair in slurry is investigated for three different initial positions. In the cases diagonal_1,coradial_1 and coaxial_14, the two 7.5 mm bubbles are positioned diagonally, co-radially and co-axially at $t = 0$ s, respectively, while the particle conditions are kept the same. The initial horizontal and vertical distances between their centers as well as particle properties are listed in Table 4. As shown in Figure 17, because of strong wake effect in the co-axial alignment, the trailing bubble catches up the leading one and stays beneath it. The coalescence occurrs at $t = 0.203$ s. In contrast, if the bubbles are aligned co-radially initially, their wakes interact with each other and tend to push the bubbles away from each other as they rise up. No coalescence between them is possible during the simulation duration of 0.3 s. In the case of diagonal alignment, the wake of the preceding bubble has still an obvious interference on the below one, although it is not located in the middle of the wake region. The trailing bubble is sucked from the side into the wake of the leading one and slides to its right side during the film drainage stage. No formation of dimple is observed and the film thickness remain almost uniform until instability begins to play a role, which is quite similar to the cases having high particle number concentrations shown above. The rupture occurs first at the upper part and then the lower part. It is interesting to see that in this case the coalescence occurs already at $t = 0.127$ s, which is much earlier compared to the co-axial case. The main reason is that the intial vertical distance between the bubbles in diagonal_1 is the half of that in the coaxial_14. As a result, it takes much longer for the trailing bubble to catch up with the leading one in the latter case. Based on the method introduced above for the determination of coalescence time, the film drainage process is longer in the diagonal alignment because of the sliding motion and orientation change. The effect of particle number concentrations on the coalescence time is similar to the co-axial case. The study shows clearly that wake is a crucial factor influencing the coalescence rate in bubble columns, which has been revealed in a number of experimental and direct numerical simulations of gas-liquid two-phase flows, e.g. Celata et al. (2004); Sanada et al. (2009); Zhang et al. (2019).

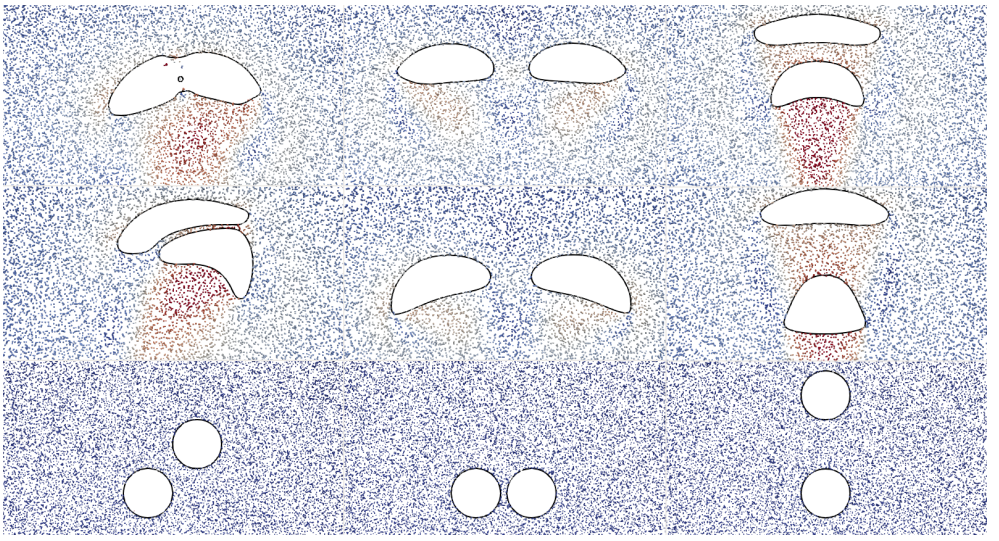

Figure 17: Effect of initial position of bubbles on their coalescence and approaching behaviour in slurry ($N_p = 8 \times 10^4$). From left to right: diagonal_1, coradial_1, coaxial_14. From bottom to top: at t=0 s, 0.1 s and 0.13 s. Particle are colored by their velocity magnitude varying from 0 to 0.3 m/s.

5. Conclusion

Understanding bubble coalescence in slurry columns and how it is affected by the particles and their properties is of great significance to numerous engineering applications. Despite decades of research high-resolution data on the film drainage process in a bubble column are scarce, which prevents a precise description of the phenomenon and derivation of reliable models and analyses. The existing work on bubble coalescence in the presence of particles either focuses on experimental or analytical study under nearly hydrostatic conditions, or is limited to mesoscopic scales, for example, acquiring the void fraction and bubble size distribution. The present work aims to fill the gap inbetween and provide insights into the film drainage process at the microscopic scale under bubble column hydrodynamic conditions. By coupling the VOF and MP-PIC methods with a chimera mesh approach, a high resolution of the interface and fluid flow field is realized and meaningful results on the effect of particle number concentration, particle size and density are achieved. The main conclusions are summarized as follows:

- The influence of particle number concentration in co-axial coalescence is complex and multimodal. At sufficiently low concentration, particles are pushed out from the film and do not alter the drainage and coalescence rate noticeably. When the concentration keeps increasing, first a physical blocking effect then a slight promotion because of the drainage changing from axisymmetry to asymmetry, is observed, and subsequently the drainage process is greatly retarded.

- The mechanism of film drainage and rupture is obviously different at high particle concentrations. For example, no dimple formation is observed, which is typical at low concentrations or in pure liquids. The drainage is largely retarded by the particles. The instability resulting in a wavy interface plays a crucial role by film rupture, and the presence of particles in the thin film affects its stability greatly.

- Both particle size and density are shown to have a dual effect in the aspects of coalescence time. Increasing of them leads to first suppression then promotion of coalescence. The results agree with the observations of the previous literature.

- Wake entrainment is proven to be a crucial factor affecting bubble coalensce in a bubble column. Whether a bubble-pair will come to collide and how long it will take to coalesce depends on their positions and surrounding hydrodynamic conditions. In the investigated parameter range and condition, the presence of particles in the

liquid is shown to affect majorly the film drainage process, while have negligible effects on the bubble rise and approach velocity.

Finally, it should be reiterated that the numerical simulation with a resolution of 0.05 *mm* is not able to capture the film rupture physically, which occurs at a scale of nanometer. The method also cannot reproduce the bouncing phenomenon as observed in many experimental and direct numerical simulation studies like Song et al. (2021); Vakarelski et al. (2019); Zhang et al. (2019). However, the objective of the study is not to predict the coalescence probability, but the film drainage behavior and the particle effects on it. The conclusion on the dual or multimodal effect of particle properties like concentration, size and density is consistent with published experimental findings.

Acknowledgements

References

Albadawi, A., Donoghue, D., Robinson, A., Murray, D., Delauré, Y., 2013. Influence of surface tension implementation in volume of fluid and coupled volume of fluid with level set methods for bubble growth and detachment. International Journal of Multiphase Flow 53, 11–28.

Ata, S., 2008. Coalescence of bubbles covered by particles. Langmuir 24, 6085–6091.

Banisi, S., Finch, J., Laplante, A., Weber, M., 1995. Effect of solid particles on gas holdup in flotation columns—ii. investigation of mechanisms of gas holdup reduction in presence of solids. Chemical Engineering Science 50, 2335–2342.

Basha, O.M., Morsi, B.I., 2018. Effects of sparger and internals designs on the local hydrodynamics in slurry bubble column reactors operating under typical fischer-tropsch process conditions-i. International Journal of Chemical Reactor Engineering 16.

Bhunia, K., Kundu, G., Mukherjee, D., 2017. Gas holdup characteristics in a flotation column with different solids. Separation Science and Technology 52, 1298–1309.

Bukur, D.B., Patel, S.A., Daly, J.G., 1990. Gas holdup and solids dispersion in a three-phase slurry bubble column. AI Ch. E. Journal (American Institute of Chemical Engineers);(United States) 36.

Caliskan, U., Miskovic, S., 2021. A chimera approach for mp-pic simulations of dense particulate flows using large parcel size relative to the computational cell size. Chemical Engineering Journal Advances 5, 100054.

Celata, G.P., Cumo, M., D'Annibale, F., Tomiyama, A., 2004. The wake effect on bubble rising velocity in one-component systems. International journal of multiphase flow 30, 939–961.

Chakraborty, I., Biswas, G., Ghoshdastidar, P., 2013. A coupled level-set and volume-of-fluid method for the buoyant rise of gas bubbles in liquids. International Journal of Heat and Mass Transfer 58, 240–259.

Chan, D.Y., Klaseboer, E., Manica, R., 2011. Film drainage and coalescence between deformable drops and bubbles. Soft Matter 7, 2235–2264.

Chen, P., Sanyal, J., Dudukovic, M., 2004. Cfd modeling of bubble columns flows: implementation of population balance. Chemical Engineering Science 59, 5201–5207.

De Swart, J., Van Vliet, R., Krishna, R., 1996. Size, structure and dynamics of "large" bubbles in a two-dimensional slurry bubble column. Chemical Engineering Science 51, 4619–4629.

Ergun, S., 1952. Fluid flow through packed columns. Chem. Eng. Prog. 48, 89–94.

Feng, J., Li, X., Bao, Y., Cai, Z., Gao, Z., 2016. Coalescence and conjunction of two in-line bubbles at low reynolds numbers. Chemical Engineering Science 141, 261–270.

Gallegos-Acevedo, P., Espinoza-Cuadra, J., Pérez-Garibay, R., Pecina-Treviño, E., 2010. Bubbles coalescence: Hydrofobic particles effect. Journal of mining science 46, 333–337.

Gandhi, B.C., 1998. Hydrodynamic studies in a slurry bubble column.

Ghani, S.A., Yaqub, R.J., Saleh, S.S., 2012. Experimental study of volumetric mass transfer coefficients in slurry bubble column reactor. J Chem Eng Process Technol 3, 10–13.

Harris, S., Crighton, D., 1994. Solitons, solitary waves, and voidage disturbances in gas-fluidized beds. Journal of Fluid Mechanics 266, 243–276.

He, X., Xu, H., Li, W., Sheng, D., 2020. An improved vof-dem model for soil-water interaction with particle size scaling. Computers and Geotechnics 128, 103818.

Hooshyar, N., Hamersma, P.J., Mudde, R.F., van Ommen, J.R., 2010. Gas fraction and bubble dynamics in structured slurry bubble columns. Industrial & engineering chemistry research 49, 10689–10697.

Horn, R.G., Del Castillo, L.A., Ohnishi, S., 2011. Coalescence map for bubbles in surfactant-free aqueous electrolyte solutions. Advances in colloid and interface science 168, 85–92.

Jamialahmadi, M., Müller-Steinhagen, H., 1991. Effect of solid particles on gas hold-up in bubble columns. The Canadian Journal of Chemical Engineering 69, 390–393.

Jing, L., Kwok, C., Leung, Y.F., Sobral, Y., 2016. Extended cfd–dem for free-surface flow with multi-size granules. International journal for numerical and analytical methods in geomechanics 40, 62–79.

Kara, S., Kelkar, B.G., Shah, Y.T., Carr, N.L., 1982. Hydrodynamics and axial mixing in a three-phase bubble column. Industrial & Engineering Chemistry Process Design and Development 21, 584–594.

Khare, A., Joshi, J., 1990. Effect of fine particles on gas hold-up in three-phase sparged reactors. The Chemical Engineering Journal 44, 11–25.

Kim, J., Lee, W., 1987. Coalescence behavior of two bubbles in stagnant liquids. Journal of Chemical Engineering of Japan 20, 448–453.

Kim, S.H., Lee, J.H., Braatz, R.D., 2020. Multi-phase particle-in-cell coupled with population balance equation (mp-pic-pbe) method for multiscale computational fluid dynamics simulation. Computers & Chemical Engineering 134, 106686.

Kim, Y., Tsutsumi, A., Yoshida, K., 1987. Effect of particle size on gas holdup in three-phase reactors. Sadhana 10, 261–268.

Kirkpatrick, R., Lockett, M., 1974. The influence of approach velocity on bubble coalescence. Chemical Engineering Science 29, 2363–2373.
Koh, P., Schwarz, M., 2006. Cfd modelling of bubble–particle attachments in flotation cells. Minerals Engineering 19, 619–626.
Krishna, R., Sie, S., 2000. Design and scale-up of the fischer–tropsch bubble column slurry reactor. Fuel processing technology 64, 73–105.
Kumar, M., Reddy, R., Banerjee, R., Mangadoddy, N., 2021. Effect of particle concentration on turbulent modulation inside hydrocyclone using coupled mppic-vof method. Separation and Purification Technology 266, 118206.
Kumar, S., Kusakabe, K., Fan, L.S., 1993. Heat transfer in three-phase fluidization and bubble-columns with high gas holdups. AIChE journal 39, 1399–1405.
Li, C., Eri, Q., 2021. Comparison between two eulerian-lagrangian methods: Cfd-dem and mppic on the biomass gasification in a fluidized bed. Biomass Conversion and Biorefinery , 1–18.
Liao, Y., Lucas, D., Krepper, E., 2014. Application of new closure models for bubble coalescence and breakup to steam–water vertical pipe flow. Nuclear Engineering and Design 279, 126–136.
Liu, B., Manica, R., Liu, Q., Klaseboer, E., Xu, Z., Xie, G., 2019. Coalescence of bubbles with mobile interfaces in water. Physical review letters 122, 194501.
Liu, J., Zhu, C., Fu, T., Ma, Y., 2014. Systematic study on the coalescence and breakup behaviors of multiple parallel bubbles rising in power-law fluid. Industrial & Engineering Chemistry Research 53, 4850–4860.
Liu, Q., Luo, Z.H., 2018. Cfd-vof-dpm simulations of bubble rising and coalescence in low hold-up particle-liquid suspension systems. Powder technology 339, 459–469.
Luo, H., 1993. Coalescence, breakup and liquid circulation in bubble column reactors. Ph.D. thesis. The Norwegian Institute of Technology.
MacKay, G., Mason, S., 1963. Some effects of interfacial diffusion on the gravity coalescence of liquid drops. Journal of Colloid Science 18, 674–683.
Maldarelli, C., Jain, R.K., 1988. The hydrodynmic stability of thin films, in: Ivanov, I. (Ed.), Thin liquid films. Marcel Dekker, INC., New York, NY, pp. 497–568.
Marrucci, G., 1969. A theory of coalescence. Chemical engineering science 24, 975–985.
Márquez Damián, S., 2013. An Extended Mixture Model for the Simultaneous Treatment of Short and Long Scale Interfaces. Ph.D. thesis. doi:10.13140/RG.2.1.3182.8320.
Mukundakrishnan, K., Quan, S., Eckmann, D.M., Ayyaswamy, P.S., 2007. Numerical study of wall effects on buoyant gas-bubble rise in a liquid-filled finite cylinder. Physical Review E 76, 036308.
Ojima, S., Hayashi, K., Tomiyama, A., 2014. Effects of hydrophilic particles on bubbly flow in slurry bubble column. International journal of multiphase flow 58, 154–167.
Omota, F., et al., 2005. Adhesion of catalyst particles to gas bubbles. Ph.D. thesis. Universiteit van Amsterdam [Host].
Ozan, S.C., Jakobsen, H.A., 2019. On the effect of the approach velocity on the coalescence of fluid particles. International Journal of Multiphase Flow 119, 223–236.
Pozzetti, G., Jasak, H., Besseron, X., Rousset, A., Peters, B., 2019. A parallel dual-grid multiscale approach to cfd–dem couplings. Journal of computational physics 378, 708–722.
Pozzetti, G., Peters, B., 2018. A multiscale dem-vof method for the simulation of three-phase flows. International Journal of Multiphase Flow 99, 186–204.
Prince, M.J., Blanch, H.W., 1990. Bubble coalescence and break-up in air-sparged bubble columns. AIChE journal 36, 1485–1499.
Rabha, S., Schubert, M., Hampel, U., 2013a. Intrinsic flow behavior in a slurry bubble column: a study on the effect of particle size. Chemical Engineering Science 93, 401–411.
Rabha, S., Schubert, M., Wagner, M., Lucas, D., Hampel, U., 2013b. Bubble size and radial gas hold-up distributions in a slurry bubble column using ultrafast electron beam x-ray tomography. AIChE journal 59, 1709–1722.
Raymond, F., Rosant, J.M., 2000. A numerical and experimental study of the terminal velocity and shape of bubbles in viscous liquids. Chemical Engineering Science 55, 943–955.
Salem-Said, A.H., Fayed, H., Ragab, S., 2013. Numerical simulations of two-phase flow in a dorr-oliver flotation cell model. Minerals 3, 284–303.
Sanada, T., Sato, Aand Shirota, M., Watanabe, M., 2009. Motion and coalescence of a pair of bubbles rising side by side. Chemical Engineering Science 64, 2659–2671.
Sarhan, A., Naser, J., Brooks, G., 2018. Effects of particle size and concentration on bubble coalescence and froth formation in a slurry bubble column. Particuology 36, 82–95.
Scheludko, A., Platikanov, D., Manev, E., 1965. Disjoining pressure in thin liquid films and the electro-magnetic retardation effect of the molecule dispersion interactions. Discussions of the Faraday Society 40, 253–265.
Snider, D.M., 2001. An incompressible three-dimensional multiphase particle-in-cell model for dense particle flows. Journal of computational physics 170, 523–549.
Song, R., Han, L., Zhang, L., Tang, S., 2021. Experiments and modeling of bubbles colliding head-on in water. AIChE Journal 67, e17220.
Spyridopoulos, M., Simons, S., Neethling, S., Cilliers, J., 2004. Effect of iiumic substances and particles on bubble coalescence and foam stability in relation to dissolved air flotation processes. Fizykochemiczne Problemy Mineralurgii/Physicochemical Problems of Mineral Processing , 37–52.
Su, X., 2005. Gas holdup in a gas-liquid-fiber semi-batch bubble column. Ph.D. thesis. Iowa State University.
Syed, A.H., 2017. Modeling of Two & Three Phases Bubble Column. Ph.D. thesis. Université de Sherbrooke.
Tavera, F., Escudero, R., 2012. Effect of solids on gas dispersion characteristics: Addition of hydrophobic and hydrophilic solids. Journal of the Mexican Chemical Society 56, 217–221.
Troshko, A.A., Zdravistch, F., 2009. Cfd modeling of slurry bubble column reactors for fisher–tropsch synthesis. Chemical engineering science 64, 892–903.
Vakarelski, I.U., Yang, F., Tian, Y.S., Li, E.Q., Chan, D.Y.C., Thoroddsen, S.T., 2019. Mobile-surface bubbles and droplets coalesce faster but bounce stronger. Science advances 5, eaaw4292.

Vandu, C., Koop, K., Krishna, R., 2004. Volumetric mass transfer coefficient in a slurry bubble column operating in the heterogeneous flow regime. Chemical Engineering Science 59, 5417–5423.

Vazirizadeh, A., 2015. The relationship between hydrodynamic variables and particle size distribution in flotation. Ph.D. thesis. Laval University.

Verma, V., Padding, J.T., 2020. A novel approach to mp-pic: Continuum particle model for dense particle flows in fluidized beds. Chemical Engineering Science: X 6, 100053.

Volkov, E.A., 1968. The method of composite meshes for finite and infinite regions with piecewise smooth boundary. Trudy Matematicheskogo Instituta imeni VA Steklova 96, 117–148.

Vrij, A., 1966. Possible mechanism for the spontaneous rupture of thin, free liquid films. Discussions of the Faraday Society 42, 23–33.

Wen, C.Y., 1966. Mechanics of fluidization, in: Chem. Eng. Prog. Symp. Ser., pp. 100–111.

Wikipedia, 2010. Multiphase particle-in-cell method. URL: https://en.wikipedia.org/wiki/Multiphase_particle-in-cell_method.

Wu, Y., Gidaspow, D., 2000. Hydrodynamic simulation of methanol synthesis in gas–liquid slurry bubble column reactors. Chemical engineering science 55, 573–587.

Xu, L., Xia, Z., Guo, X., Chen, C., 2014. Application of population balance model in the simulation of slurry bubble column. Industrial & Engineering Chemistry Research 53, 4922–4930.

Zhang, J., Chen, L., Ni, M., 2019. Vortex interactions between a pair of bubbles rising side by side in ordinary viscous liquids. Physical Review Fluids 4, 043604.

Zhang, X., 2017. Study of thin liquid film drainage in bubble-liquid-solid systems using integrated thin liquid film force apparatus (ITLFFA). Ph.D. thesis. University of Alberta.